CONTROL OF TWO WHEEL SELF STABILIZING MOBILE ROBOT WITH A SIMPLE ARM

A MASTER'S THESIS

in

Mechatronics Engineering

Atilim University

by

SERTAÇ EMRE KARA

OCTOBER 2014

CONTROL OF TWO WHEEL SELF STABILIZING MOBILE ROBOT WITH A SIMPLE ARM

A THESIS SUBMITTED TO

THE GRADUATE SCHOOL OF NATURAL AND APPLIED SCIENCES

OF

ATILIM UNIVERSITY

BY

SERTAÇ EMRE KARA

IN PARTIAL FULFILLMENT OF THE REQUIREMENTS FOR THE DEGREE OF

MASTER OF SCIENCE

IN

THE DEPARTMENT OF MECHATRONICS ENGINEERING

OCTOBER 2014

Approval of the Graduate School of Natural and Applied Sciences, Atılım University.

_____

Prof. Dr. K. İbrahim AKMAN

Director

I certify that this thesis satisfies all the requirements as a thesis for the degree of Master of Science.

_____

Prof. Dr. Abdulkadir ERDEN

Head of Department

This is to certify that we have read the thesis "Control of Two Wheel Self Stabilizing Mobile Robot with a Simple Arm" submitted by "Sertaç Emre Kara" and that in our opinion it is fully adequate, in scope and quality, as a thesis for the degree of Master of Science.

Asst. Prof. Dr. Bülent İrfanoğlu	Asst. Prof. Dr. Kutluk Bilge Arıkan
Co-Supervisor	Supervisor

Examining Committee Members

Assoc. Prof. Dr.Fuad Aliew	_____
Assoc. Prof. Dr. Sedat Nazlibilek	_____
Asst. Prof. Dr. Hakan Tora	_____
Asst. Prof. Dr.Bulent Irfanoglu	_____
Asst. Prof. Dr.Kutluk Bilge Arıkan	_____

Date: (20.10.2014)

I declare and guarantee that all data, knowledge and information in this document has been obtained, processed and presented in accordance with academic rules and ethical conduct. Based on these rules and conduct, I have fully cited and referenced all material and results that are not original to this work.

Sertaç Emre KARA

Signature:

ABSTRACT

CONTROL OF TWO WHEEL SELF STABILIZING MOBILE ROBOT WITH A SIMPLE ARM

Kara, Sertaç Emre

M.S., Mechatronics Engineering Department

Supervisor: Asst. Prof. Dr. Kutluk Bilge Arıkan

Co-Supervisor: Asst. Prof. Dr. Bülent İrfanoğlu

October 2014, 66 pages

In this thesis mechanical and electronic structure of two wheeled inverted pendulum robot with a simple arm studied. Also design and implementation of coefficient diagram method (CDM) is covered. Mechanic and electronic structure is designed and manufactured in terms of mechatronics engineering. To sense the body pitch angle one degree of freedom inertial measurement unit (IMU) designed. Arm of the robotic platform is examined in simulations and in real time experiments. Arms obtain external disturbance and maintain stability in controller simulations. In real time experiments stability performance of CDM controller studied. The system is maintained stability in pitch angle and linear displacement while external and internal (arms effect) disturbances applied.

Keywords: CDM, Two Wheeled Inverted Pendulum, Stabilization, DsPic Blokset for Matlab Simulink

ÖZ

TEK KOLLU İKİ TEKERLEKLİ KENDİNİ DENGELEYEN GEZER ROBOTUN DENETİMİ

Kara, Sertaç Emre

Yüksek Lisans, Mekatronik Mühendisliği Bölümü

Tez Yöneticisi: Yrd. Doç. Dr. Kutluk Bilge Arıkan

Ortak Tez Yöneticisi: Yrd. Doç Dr. Bülent İrfanoğlu

Ekim 2014, 66 sayfa

Bu tezde tek bir kol ile desteklenmiş iki tekerlekli ters sarkaç robotunun mekanik ve elektronik yapısı çalışılmıştır. Ayrıca katsayı diagram metodunun (KDM) tasarımı ve uygulanması ele alınmıştır. Mekanik ve elektronik yapı mekatronik mühendisliği açısından tasarlanıp üretilmiştir. Sistemin eğim açısını ölçmek için tek serbestlik dereceli ataletsel ölçüm birimi (AÖB) tasarlanmıştır. Robotik platformun kolları simülasyonda ve gerçek zamanda incelenmiştir. Kollar simülasyonda harici bozucu etkenleri oluşturmak ve dengelemeye yardımcı olmak için kullanılmıştır. Gerçek zamanda KDM denetimcinin kararlılık verimliliği çalışılmıştır. Sisteme gerçek zamanda harici bozucu ve dahili bozucu etken (kolun etkisi) uygulanırken, KDM denetimcisi sistemin açısal dengesini ve doğrusal yer değiştirmesini sağlamaktadır.

Anahtar Kelimeler: KDM, İki Tekerlekli Ters Sarkaç, Kararlılık, Matlab Simulink için DsPic Araç Kutusu

To My Family

ACKNOWLEDGMENTS

I express sincere appreciation to my supervisor Asst. Prof. Dr. Kutluk Bilge Arıkan for his guidance and insight throughout the research. Thanks also go to my cosupervisor Asst. Prof. Dr. Bülent İrfanoğlu. The technical and mental assistance of Mohammad Hassan Golmohammad Zadeh, Ayça Göçmen, Emre Güner Cahit Gürel, Meral Aday, Handan Kara and technicians are gratefully acknowledged.

TABLE OF CONTENTS

ABSTRACT iii

OZ iv

DEDICATION v

ACKNOWLEDGMENTS vi

TABLE OF CONTENTS vii

LIST OF TABLES ix

LIST OF FIGURES xi

LIST OF ABBREVIATIONS xii

CHAPTER

1. INTRODUCTION 1

1.1 Background 1

1.2 Aim of the Thesis 3

1.3 Chapter Organization 4

2. LITERATURE SURVEY 5

3. SYSTEM COMPONENTS 13

3.1 Mechanical Structure 13

3.2 Electronics 14

3.2.1 Controller Card with Microchip DSPIC 30F4011 Microcontroller 15

3.2.2 Pololu VNH3SP30 Motor Driver Carrier MD01B 16

3.2.3 Xbee 2mW Series 2(ZB) 16
3.2.4 Pololu D15V70F5S3 5 V Regulator 18
3.2.5 DC Motor and Encoder 18
3.2.6 Li-po battery 20
3.2.7 Savöx SH-1290MG Servo Motor 20
3.3 Single DOF IMU 21
3.3.1 Test Bench 21
3.3.2 Estimators 23
3.3.3 Complimentary Filter 23
3.3.4 Kalman Filter 25
3.3.5 Optimization of Filter Parameters 27
4. MATHEMATICAL MODELLING 33
4.1 State Space Representation 37
5. CONTROLLER DESIGN AND SIMULATIONS 39
5.1 CDM Concept 40
5.2 Controller Design 41
5.3 Simulations 45
5.3.1 First Condition: Arm is not Affecting to Disturbance Rejection 45
5.3.2 Second Condition: Arm is Affecting to Disturbance Rejection 48
6. REAL TIME EXPERIMENTS 55
6.1 Controller Software 56
6.2 Real Time Experiments Without Disturbance 57
6.3 Real Time Experiments with 50 g Loaded Arm is Affecting as Disturbance .. 58
7. DISCUSSIONS AND CONCLUSIONS 59

LIST OF TABLES

Table 1: Motor Driver Specifications 16
Table 2: Xbee Specifications 17
Table 3: DC motor Specifications 19
Table 4: Encoder Specifications 19
Table 5: Servo Motor Specifications 20
Table 6: Utilized Variations of CF 24
Table 7: Utilized Variations of KF 26
Table 8: Parameters of the System 36
Table 9: Rank of the $\mathbf{A}_a$ 43
Table 10: Parameters of the CDM 44
Table 11: Poles of the both system 44
Table 12: $\mathbf{K}_a$ Values 45

LIST OF FIGURES

Figure 1: The illustration of TWMR 2
Figure 2: Segway HT 5
Figure 3: The Segway RMP 6
Figure 4: MIT's Cardea with kickstand extended. 6
Figure 5: The NASA Robonaut RMP 6
Figure 6: CMU's soccer-playing RMP 7
Figure 7: USC's RMP 8
Figure 8: JOE 8
Figure 9: uBOT 8
Figure 10: Ballbot with arms, Carnige Mellon University 8
Figure 11: Mobile Manipulator by Cihan Acar 9
Figure 12: Golem Krang 10
Figure 13: Side and Front View of TWMR 13
Figure 14: Side and Front View of TWMR 14
Figure 15: Main Controller Scheme of the system 15
Figure 16: Robot programming Scheme 16
Figure 17: Pololu VNH3SP30 Motor Driver Carrier MD01B 16
Figure 18: Xbee Series 2 and USB Dongle 17
Figure 19: Operational Scheme of Xbee RF Transmission 17
Figure 20: Pololu D15V70F5S3 Regulator 18
Figure 21: HN-GH12-1634T-30:1 DC motor 18
Figure 22: US Digital E4P Miniature Optical Encoder 19
Figure 23: THK 11.1 V Li-Po Battery 20
Figure 24: Savöx SH-1290MG Servo Motor 20
Figure 25: IMU test Bench 22
Figure 26: Detailed Schematic of the Test Bench 22
Figure 27: Complimentary Filter Scheme 23

Figure 28: Complementary Filter in Simulink 24
Figure 29: Kalman Filter in Simulink 26
Figure 30: Actual Angular Position 27
Figure 31: Accelerometer Measurement 28
Figure 32: Gyro Measurement 28
Figure 33: Actual Position and Standard CF Estimation 29
Figure 34: Actual Position and Estimation of CF with Different Cut-off Frequencies 29
Figure 35: Actual Position and Estimation of Weighted CF 30
Figure 36: Actual Position and Estimation of Weighted CF with Different Cut-off Frequencies 30
Figure 37: Actual Position and Estimation of Standard KF 31
Figure 38: Actual Position and Estimation of Weighted KF 31
Figure 39: Actual Position and Estimation of fused CF and KF 32
Figure 40: FBD of the System 33
Figure 41: DC motor model 35
Figure 42: Block Diagram of Augmented System 42
Figure 43: Simulink view of condition with no disturbance exists 45
Figure 44: Sinusoidal reference, input voltage, pitch angle with no disturbance results 46
Figure 45: Square reference, input voltage, pitch angle with no disturbance results. 46
Figure 46: Simulink view of condition with disturbance exists 47
Figure 47: Sinusoidal reference, input voltage, pitch angle and disturbance 47
Figure 48: Square reference, input voltage, pitch angle and disturbance 48
Figure 49: Simulink view of condition with arm and there is no disturbance exists . 48
Figure 50: Sinusoidal reference, DC motor input voltage, Rc servo input torque pitch angle, arm angle with there is no disturbance exists 49
Figure 51: Square reference, DC motor input voltage, Rc servo input torque pitch angle, arm angle with there is no disturbance exists 50
Figure 52: Simulink view of condition with arm and there is disturbance exists 51
Figure 53: Sinusoidal reference, DC motor input voltage, Rc servo input torque, pitch angle, arm angle and disturbance 51
Figure 54: Sinusoidal reference, DC motor input voltage, Rc servo input torque, pitch angle, arm angle and disturbance 52

Figure 55: Disturbance Applied to system 53
Figure 56: Comparison of body pitch angle 53
Figure 57: Comparison of linear position 54
Figure 58: Comparison of power 54
Figure 59: DsPic Blockset for Matlab Simulink 56
Figure 60: Simulink scheme of CDM Contoller 56
Figure 61: Zero reference without arm disturbance in real time 57
Figure 62: Sinusodial type reference without arm disturbance in real time 57
Figure 63: Zero reference with 50 g loaded arm affecting as disturbance in real time 58
Figure 64: Sinusodial type reference with 50 g loaded arm affecting as disturbance in real time 58

LIST OF ABBREVIATIONS

A/D	-	Analog/Digital
CDM	-	Coefficient Diagram Method
CF	-	Complimentary Filter
COG	-	Center of Gravity
COM	-	Center of Mass
DC	-	Direct Current
DSP	-	Digital Signal Processing
DOF	-	Degree of Freedom
FBD	-	Free Body Diagram
EMF	-	Electromotive Force
HT	-	Human Transporter
IEEE	-	The Institute of Electrical and Electronics Engineers
IMU	-	Inertial Measurement Unit
I/O	-	Input/Output
KF	-	Kalman Filter
Li-po	-	Lithium – Ion Polymer
LQR	-	Linear Quadratic Regulator
MEMS	-	Micro Electro Mechanical Systems
MIPS	-	Millions of instructions per second
PC	-	Personal Computer
PCI	-	Peripheral Component Interconnect

PIC	-	Programmable Interface Controller
PID	-	Proportional Integral Derivative
PWM	-	Pulse Width Modulation
RF	-	Radio Frequency
RMP	-	Robotic Mobility Platform
RTWT	-	Real Time Windows Target
TWMR	-	Two Wheeled Manipulator Platform
UART	-	Universal asynchronous transmitter/receiver
USB	-	Universal Serial Bus

NOMENCLATURE

θ	-	Angular position of body
$\dot{\theta}$	-	Angular velocity of body
$\ddot{\theta}$	-	Angular acceleration of body
β	-	Angular position of wheel
$\dot{\beta}$	-	Angular velocity of wheel
$\ddot{\beta}$	-	Angular acceleration of wheel
α	-	Angular position between arm and body
$\dot{\alpha}$	-	Angular velocity between arm and body
$\ddot{\alpha}$	-	Angular acceleration between arm and body
φ	-	Angular position between arm and vertical plane
χ	-	Linear displacement in x direction
$\dot{x}$	-	Linear velocity in x direction
$\ddot{x}$	-	Linear acceleration in x direction
x_a	-	Linear displacement of COM of body in x direction
$\dot{x}_a$	-	Linear velocity of COM of body in x direction
x_b	-	Linear displacement of COM of arm in x direction
$\dot{x}_b$	-	Linear velocity of COM of arm in x direction
y_a	-	Linear displacement of COM of arm in y direction
$\dot{y}_a$	-	Linear velocity of COM of arm in y direction

y_b	-	Linear displacement of COM of body in y direction
$\dot{y}_b$	-	Linear velocity of COM of body in y direction
V_e	-	Terminal voltage
V_a	-	Voltage applied
Kt	-	Torque Constant
Ke	-	Back EMF constant
R	-	Terminal resistance of DC motor
n	-	Gear ratio
l	-	Motor Inductance
i	-	Motor armature current
r	-	Wheel Radius
H_1	-	Distance between wheel center and COM of body
H_2	-	Distance between joint of arm to COM of arm
d	-	Length of body
g	-	Gravitational acceleration
M_a	-	Mass of arm
M_w	-	Mass of wheel
M_b	-	Mass of body
J_a	-	Moment of inertia of arm
J_b	-	Moment of inertia of body
J_w	-	Moment of inertia of wheel

b_0 - Friction between wheel and ground

b_1 - Friction between body and wheel

b_2 - Friction between body and arm

CHAPTER 1

INTRODUCTION

1.1 Background

Mobile robotics is one of the most under-researched topics in recent century. There are wheeled human transporters, wheeled space robots, industrial robots etc. which can work complete autonomous and fulfill hazardous and dangerous tasks. However under actuated mobile robots are still under-development and researchers trying to make them perfect. There are under actuated robots with wheel and walking gait. Walking robots are good for human service and rough terrain with manual control or semi-automatic. They have superior maneuver but they are very slow. These robots are used in civil and military applications.

Two wheeled systems are designed for human transportation at the beginning. But in the last decade two wheeled systems are built for mobile robotics applications as mapping, industrial carriers, servant robots and etc. To give more flexibility and freedom, these two wheeled systems are combined with manipulators thus mobile manipulators come around. Mobile manipulator can achieve many task as obstacle avoidance, pushing, picking and placing etc. Walking robots can also achieve these kind of tasks but their complex structure restricts usage most of the cases. These wheeled part and manipulator are constructing a hybrid platform. Hybrid platforms can mimic the biological creatures like insects and animals. These platforms make us understand the posture stability and complex control techniques.

In these thesis two wheeled under actuated robot is developed. There is an arm added to give additionary freedom. Hence *Two Wheeled Manipulator Robot* (TWMR) constructed. This arm can be used as a manipulator and disturbance source. Arm source also can be effective for posture stability.

TWMR designed to be two arms at the beginning. Since the platform modelled to move one direction i.e. the system can move in two dimensions, arms reduced to one arm on the chest (shown in Figure 1). The system has different functions in the mathematical model and the real system. In the mathematical model arms have two different functions. First function is to create disturbances while the controller strives for balancing and linear movement. Second function is to help balancing when there is an external disturbance effects or when the initial conditions are non-zero.

In real system arm is used for creating disturbances. The realization of the system has some complications. The arm motor chosen to be RC servo motor. Since the controller is linear state feedback based, all the state variables have to be observed. Unless RC servo motor has no feedback. Hence In real system arm is a source of disturbance when the task is to carry weight Platform expected to eliminate external disturbances.

Figure 1: The illustration of TWMR

In order to obtain pitch angle of the TWMR one degree of freedom inertial measurement unit (IMU) designed. IMU consist of one degree of freedom gyro and accelerometer. Complimentary filter algorithm used to achieve sensor fusion which ensures the optimum filter parameters of the sensor set.

TWMR's mathematical model derived with *Lagrange-Euler Method. S*ystem is controlled with *Coefficient Diagram Method* (CDM) which is a linear polynomial control method. All the control system design for linear time invariant dynamic

system boils down to proper selection of the characteristic polynomials and proper selection of numerator polynomials for concerned input-output relations. When these polynomials are properly selected, the design of controller transfer function is straight forward, and requires only simple mathematics. The proper selection of the characteristic polynomial is not difficult, if only stability and response are to be satisfied, but it becomes complicated when robustness issue is presented. The coefficient diagram method (CDM) is an answer to this problem.

1.2 Aim of the Thesis

TWMR is designed as a mobile manipulator which satisfies robustness criterion with CDM controller explained by Shunji Manabe. Manipulator has two main tasks to achieve. One of the task is to balance itself with the aid of arms with state feedback controller which has parameters found from CDM method. Second task is using arm as a disturbance source. Therefore mathematical models are derived and two tasks are simulated with Matlab-Simulink.

Robotic platform is designed in mechatronic engineering perspective. The platform is two dimensional motion capability. To obtain pitch angle one dimensional IMU designed and built. Two DC motors are used to drive two wheels. Wheels are produced by 3D printer and covered with rubber to attain more friction. Arms are reduced to one arm because of the reasons explained above. Hence one RC servo motor is used. To control all these components a controller unit designed which has Microchip dsPIC30f4011 microcontroller. Controller system programmed with Microschip Pickit 3. To complete all the controller tasks Matlab simulink blocksets for Microchip microcontrollers is used as a software.

In real-time works arms are used as a disturbance source only. CDM controller eliminate external disturbance and internal disturbances at the same time. Two state variables which is pitch angle and linear displacement is controlled while the disturbances are effecting the platform.

1.3 Chapter Organization

Literature Survey explained in **Chapter 2**. Mechanical and electronic components introduced in **Chapter 3**. Mathematical model derived and state space representation given in **Chapter 4**. CDM controller is introduced and controller parameters are obtained in **Chapter 5**. Controller software introduced and real time experiment result given in. **Chapter 6**. Discussions and conclusions are explained in **Chapter 7.**

CHAPTER 2

LITERATURE SURVEY

Two wheeled robotic systems has wide range of research and application fields. Most famous commercial robotic vehicle, Segway self-balancing human transporter (HT) is a robust and agile robotic vehicle in the last decade (shown in Figure 2). These vehicles with two wheel has a zero turning point that is good advantage in small areas.

Figure 2: Segway HT, [6]

Segway also designed a different concept of robotic vehicle known as robotic mobile platform (RMP). The Segway RMP is faster, cheaper, and more agile than existing comparable platforms. It is also rugged, has a small footprint, a zero turning radius, and yet can carry a greater payload. Controller of the RMP is choosen to be LQR. Feedback controller can tolerate plant variation (that is the point of feedback after all), a basic LQR controller for a balancing machine does not produce the same balancing dynamics regardless of payload. Thus the controller must be matched to the mass properties of the RMP (inertia, mass, center of gravity). Because of system loading, there was really only 1-2 KB of program memory available for the balancing controller. As a result, more elaborate adaptive schemes were not tried.[6]

Figure 3: The Segway RMP,[6]

Cardea [11] in Figure 4 and NASA's Robonaut [9] in Figure 5 that use the Segway RMP (shown in Figure 3) for the mobile platform are examples of two-wheeled dynamically stable mobile manipulation systems. Although these systems have many advantages with respect to conventional statically stable mobile manipulators, due to dynamical stability they require an active control mechanism to maintain their balance and pose.

Figure 4: MIT's Cardea with kickstand extended.[8]

Figure 5: The NASA Robonaut RMP.[8]

Capitalizing on the RMP's human-like size, weight, and balancing ability, CMU is using Segway RMPs and HTs to create a new domain for studying human-robot interaction in peer-based teams, namely Segway Soccer [12] (shown in Figure 6). Each team would probably include two units of each type. The RMP is ideally suited to this domain since its dynamic balancing gives the robot a measure of active compliance very useful when collisions occur.[13] CMU's research effort with the RMP over the last year has focused on building the individual capabilities a robot

needs to operate autonomously within a soccer-playing team, including: *ƒ* Developing real-time, robust, and adaptable vision algorithms: the only additional sensor added to the RMP for soccer playing was a color Web camera; the color blob extracting CMVision library was extended to detect contrasting objects under variable illumination conditions; Developing ball manipulation hardware: a pneumatic kicking mechanism was designed to impart maximum energy to the ball; Developing robust multi-object tracking techniques with real-time implementations: including efficient recognition of the multiple objects relevant to the human-robot game, namely the ball, the goals, the field markers, and the other robot and human teammates and opponents; *ƒ* Developing skill-learning algorithms: to eliminate the time-consuming and error-prone process of tuning individual skills, a skill recording system was developed, whereby a human operator guides the robot via tele-operation through a complex motion, with the robot commands recorded to a file that can be later played back as an acquired skill.[14]

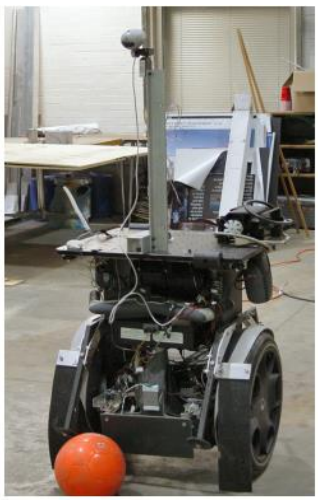

Figure 6: CMU's soccer-playing RMP, [12]

The University of Southern California's Robotics Research Lab has used the Segway RMP as a platform for research in mapping, localization, stealthy navigation, and path planning (shown in Figure 7). For experiments in 3D navigation and mapping of outdoor urban environments, the RMP was equipped with one SICK ladar in the horizontal plane and one or more ladars in the vertical plane. The RMP was selected for this task because of its speed, endurance, large payload capacity, and high vantage point for sensors, which helped eliminate ground clutter.[15]

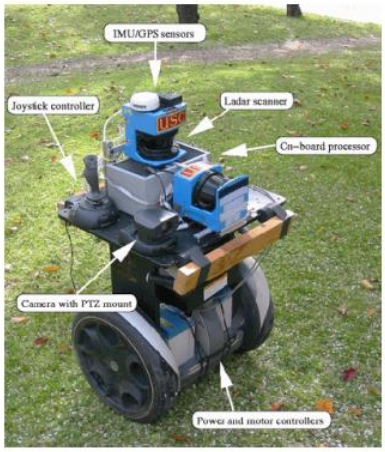

Figure 7: USC's RMP,[15]

There also other robotic platforms like JOE [16] in Figure 8, uBot [17, 19] in Figure 9 and Ballbot [18] in Figure 10 can be listed. uBot especially built firstly as swarm application then it is reconstructed for mobile manipulator.

Figure 8: JOE,[16]

Figure 9: uBOT, [17,19]

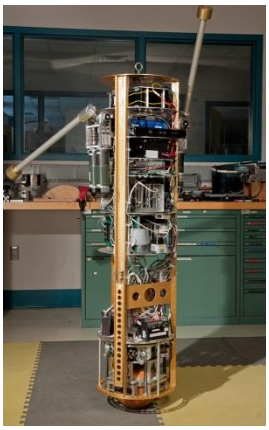

Figure 10: Ballbot with arms, Carnige Mellon University

Mobile manipulators have been recently studied in different applications. A mobile manipulator has a multiple degree of freedom that makes the whole system more robust and improve the system to gain more movement capability. The main concept is to combine a robotic arm or manipulator in to a mobile base. The advantage of the mobile manipulation come from the mobility and large workspace of the mobile platform and dexterity manipulation and many degrees of freedom of the manipulator part.

A mobile manipulator can be explained as a combination of links connected together by active or passive joints. The main application area of these robots are factories and industrial environments where they are capable of performing tasks such as welding, assembly, painting, polishing, grinding. The previous researches related to these kinds of systems mostly focus on the improvement of performance, accuracy, and speed. These kinds of manipulators have limitations due to their fixed based structures. It is possible to increase the workspaces of the manipulators robots by combining them with mobile type robots. [1, 2, 3]

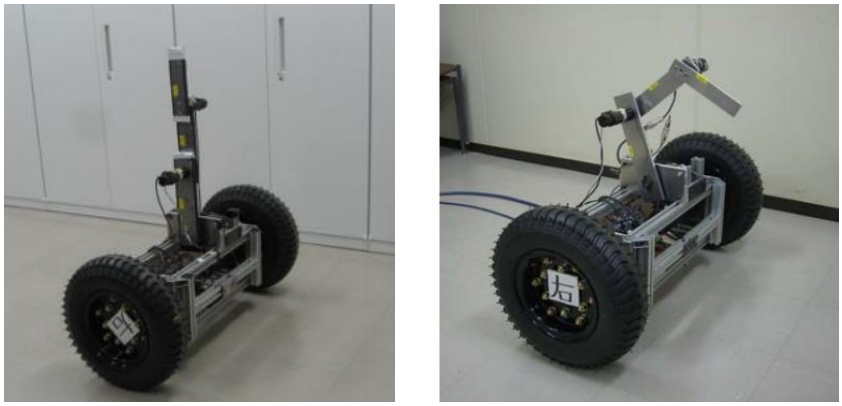

Figure 11: Mobile Manipulator by Cihan Acar [1]

Mobile robots are mobile platforms that are not connected the fixed location. They have high mobility and are suitable to be used in environments where there is not a fixed structure. Transportation, navigation, guidance, cooperation are some of the usage areas of these types of robots. The combination of mobile robots and manipulators form the mobile manipulators that have properties of both types of robots (shown in Figure 11). Since mobile manipulators have many degrees of freedom, they are able to perform many tasks such as avoidance of obstacles, pushing, picking and placing task, opening doors, etc. Even though bipedal robots are also capable of performing these kinds of tasks and are more suitable for cases like climbing stairs, their complex structure restricts their usage in most of these cases. The precise locomotion of these systems requires high degrees of freedom in their legs, which increase the total mass and complexity of the system and also restrict the degrees of freedom used for the dexterous manipulation. Wheel robots have less complex structures and are easier to control with regard to the legged type robots. [1, 2, 3, 4, 5]

Two-wheeled mobile manipulators without any caster consist of a two-wheeled mobile platform and a manipulator. These systems are dynamically stable unlike the conventional mobile manipulators as described above. They have smaller wheelbase than the statically stable mobile manipulator. They are also more flexible and maneuverable with respect to the statically stable mobile manipulators. It is possible to control the orientation of these types robots, which can be utilized to improve the force generation of ability of the manipulator. [10] In addition, they are able to tolerate unexpected external forces due to their dynamic stability. For instance, when an external force in the lateral direction is applied the robot, it is enforced to change its position in order to maintain its stability. This behavior is similar to the compliance motion, which decreases the impact force and the damage received by the system. [8] As a result, these systems can be used easily in the human environment for human assistance.

Another interesting study is Golem Krang Designed at Georgia Tech (shown in Figure 12). This robot is designed for service applications. Its anthropomorphic structure, with two arms and a two-DOF torso, is designed to store energy and utilize momentum in order to perform heavy tasks that match and exceed human capabilities [20, 21].

Figure 12: Golem Krang, [21]

There are different type of controllers used in these robots such as LQR. Nevertheless to implement these kind of controller mathematical model should be

linearized.[22, 23, 24, 25, 26, 27, 28, 29, 30, 31] In some applications State and disturbance observer also can be used. [1, 2, 3, 22, 23, 24 , 25, 26, 27]. Observer is used in order to estimate the states in [22, 46]. Many studies apply Lagrange equations while deriving mathematical model [22, 25, 28]. But in some works Newton's law used to derieve mathematical model [32, 33, 34, 35]. System's states are determined as linear displacement and linear velocity in longitudinal direction, angle and angular rate related to pitch dynamics [32, 36].

Mathematical model is the representation of the real system. Therefore, system's parameters such as inertia are important in order to make model more accurate. Inertia of the system is determined by calculating as in [43, 44] or testing as in [25, 38]. Designing controller is the crucial part of the system. The main problem stability is satisfied by the controller. Although this system is highly non-linear, linear controllers are generally applied to the system after linearization because of its low cost and less complexity. However, non-linear controllers are also attempted in [30]. Most of the studies focus on auto-balancing control. Besides auto-balancing control, controllers are used for tracking control in some studies as [29, 42, 46].
The goal is to drive the error between the reference and the output to zero [52]. Error space approach based control systems which have a difference of having integral of the error term as a state is applied on several systems in path tracking systems. Other control systems are used in the path tracking also. backstepping type controllers are the most preferred controllers in path tracking applications in the literature [49, 50, 51].

H_2 and H_{inf} methods are used in [47] and [48], respectively. Other controller methods implemented on the system are fuzzy control as in [46, 53, 54] and adaptive control in [45, 55, 56]. A nonlinear sliding mode control is one of the robust controller described in [56].

The essential aim is to stabilize pitch angle in the system. Thus, necessary data must be taken from sensors. The main sensors of the system are accelerometer and gyroscopes which measure the angle and angular rate of the body, respectively. Most of the studies, [57, 58, 59] use both of these sensors together.

In control system design system components such as sensors, actuators and controllers are important. However design theory is the most important part of the components because it affects the controller. To design linear time invariant systems selection of characteristic polynominals are important. Proper selection of coefficents of feedback gain matrix is hard to determine. CDM method is a robust method that make this selection easier [60, 61, 62].

Lastly to the nonlinear controller, a linear controller is easier to be designed and implemented. A linear augmented controller with an integrator can satisfy the design specification. The integrator is needed to reject the steady-state error in controlling the inverted pendulum system due to the hardware of the system. Unfortunately the choice of the weighting matrix was still trial and error [63, 64, 65].

CHAPTER 3

SYSTEM COMPONENTS

3.1 Mechanical Structure

Body main frame constructed from aluminum profile and plexiglass carrier. All electronics assembled on the plexiglass carrier (shown in Figure 13). Wheel part constructed from ABS plastic with 3D printer and covered with thin rubber layer to obtain more friction. Arm is manufactured from 6 mm plexiglass layer which has and slot at the end to be assembled weight.

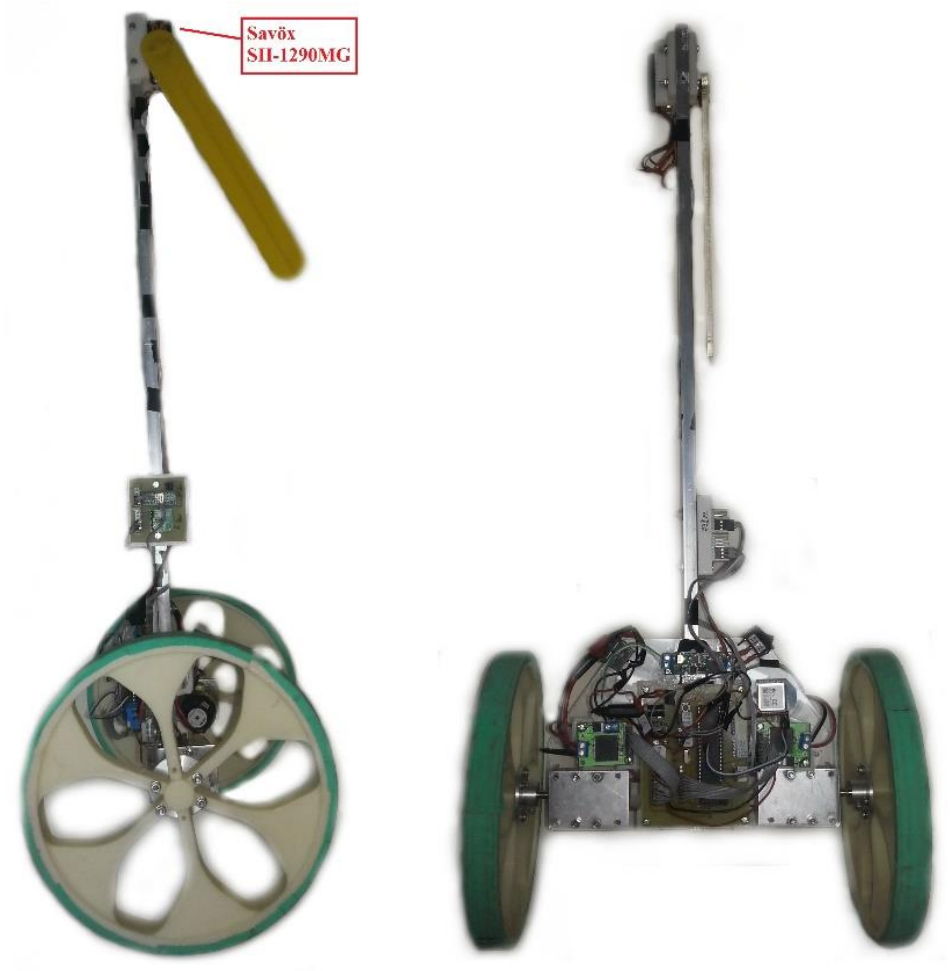

Figure 13: Side and Front View of TWMR

3.2 Electronics

The electronics components used in the system listed below which are shown in Figure 14:

- Controller Card with Microchip DsPic 30F4011 microcontroller
- Pololu motor driver
- Xbee RF transmitter/receiver
- 5V DC regulator
- Single DOF IMU
- 11.1 V Li-Po battery
- DC motor and encoder
- Savöx SH-1290MG Servo Motor

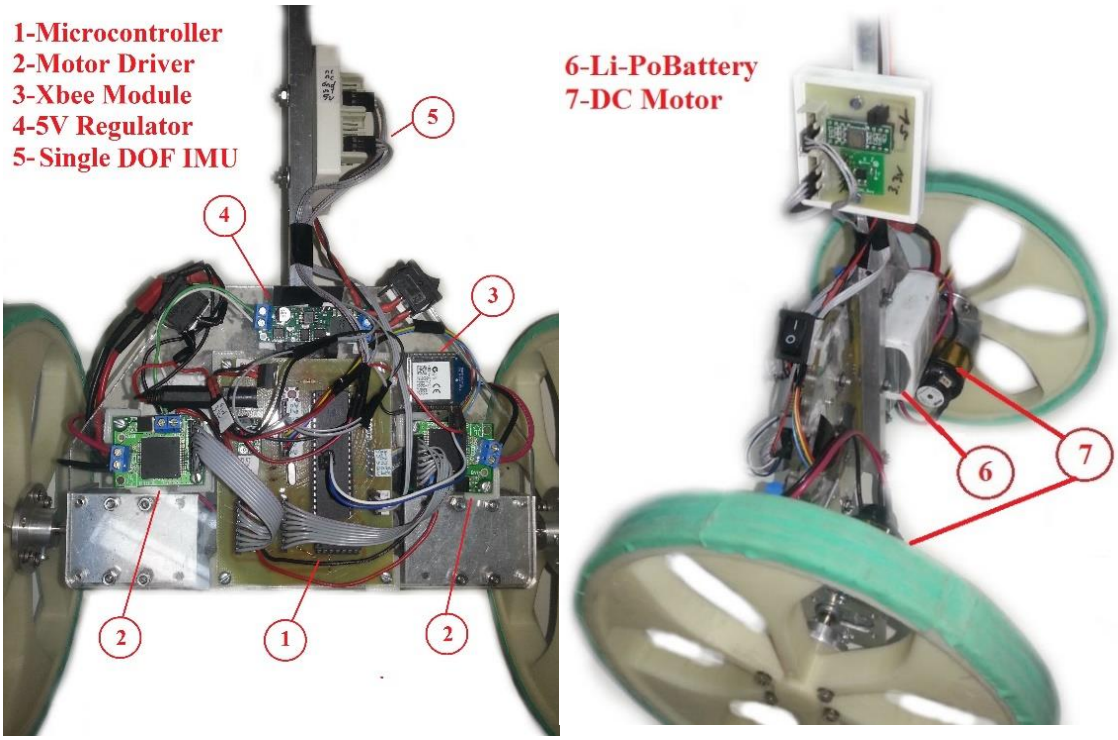

Figure 14: Side and Front View of TWMR

The main controller part is designed and manufactured on PCB. Microcontroller embedded on the system is chosen in terms of affordability and effectiveness.

Data acquisition performed with Xbee RF transmitter/receiver by serial communication protocol.

3.2.1 Controller Card with Microchip DSPIC 30F4011 Microcontroller

A controller board is produced by using Microchip Dspic 30F4011 Microcontroller. All electronic components are soldered on the PCB board. General Control scheme is shown in Figure 15. Dspic Microcontroller running speed is set to 40 MIPS by changing oscillator setting to PLL16.

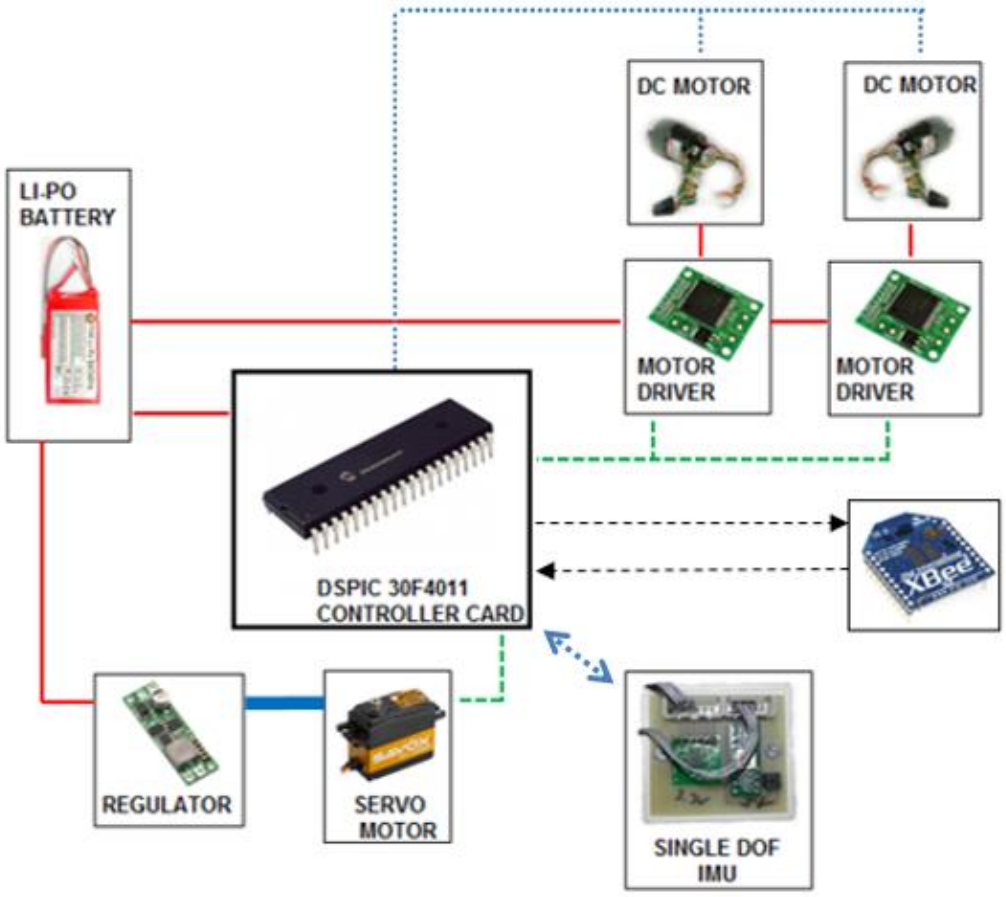

Figure 15: Main Controller Scheme of the system

Microchip pic kit 3 is used to program controller board. Pic kit 3 is smart and compact programmer. There is a button to program multiple PICs in sequence. Pic kit 3 is connected to PC via USB cable as shown in Figure 16.

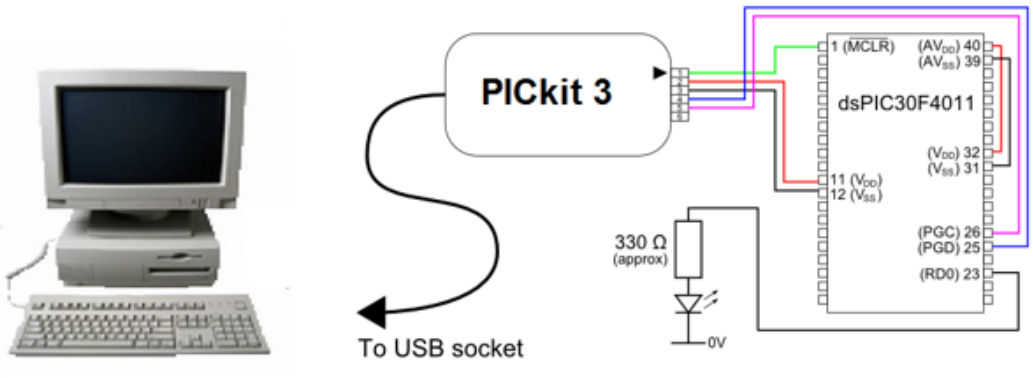

Figure 16: Robot programming Scheme

3.2.2 Pololu VNH3SP30 Motor Driver Carrier MD01B

Each motor has been driven by using presented motor drivers shown in Figure 17.

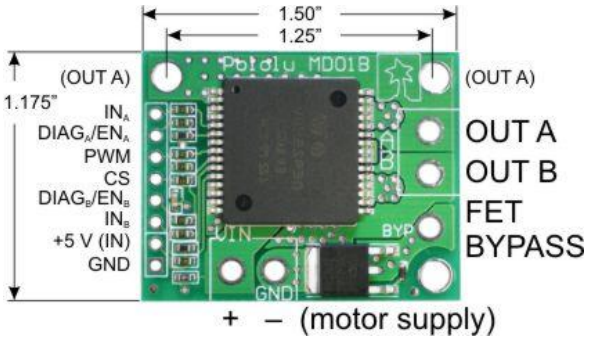

Figure 17: Pololu VNH3SP30 Motor Driver Carrier MD01B

Table 1: Motor Driver Specifications

PARAMETER	SPECIFICATION
Operating Voltage	**5.5-16 V**
Max PWM Frequency	**10 kHz**
Current for infinite run time	**9 A**
Peak Current	**30 A**

3.2.3 Xbee 2mW Series 2(ZB)

Xbee has a wide range of application area in mechatronic engineering. Xbee uses serial communication protocol that makes users benefit.

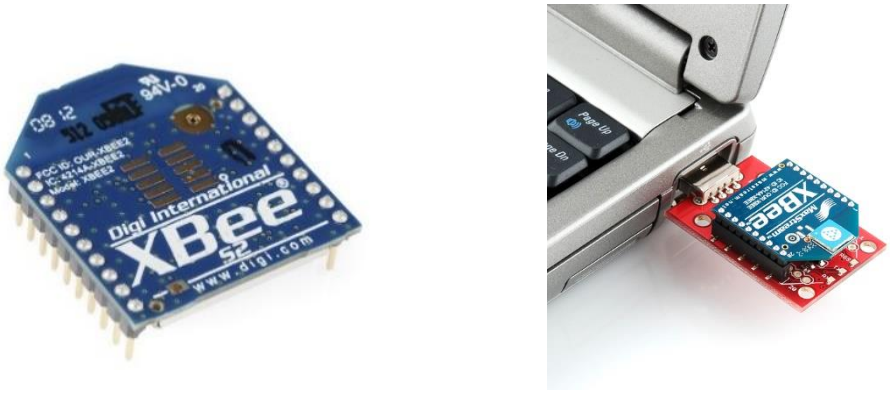

Figure 18: Xbee Series 2 and USB Dongle

Xbee used with USB Dongle (shown in Figure 18) connected to PC to collect Data. Matlab RTWT serial communication blocks is used as software part of data acquisition. Another Xbee module is implemented on the robot to transmit sensor and encoder data. Concept of operation of data transmission between robot and PC shown in Figure 19.

Table 2: Xbee Specifications

PARAMETER	SPECIFICATION
Operating Voltage	**3.3 V**
Operating Current	**40 mA**
Range	**120 m**
Data Rate	**250 kbps**

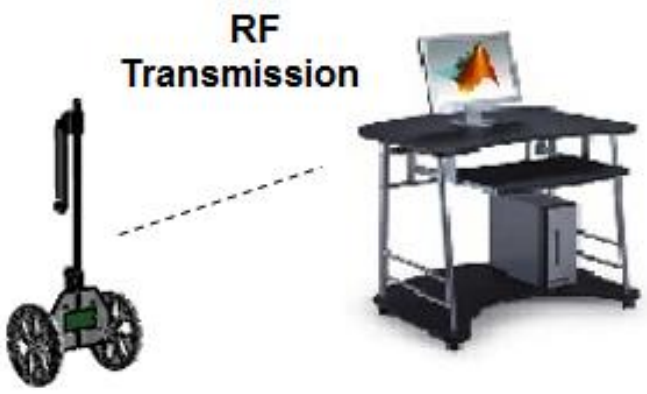

Figure 19: Operational Scheme of Xbee RF Transmission

3.2.4 Pololu D15V70F5S3 5 V Regulator

These buck (step-down) voltage regulator (shown in Figure 20) generate lower, user-selectable output voltages from an input voltage range of 4.5 to 24 V. Typical continuous output current is 7 A. This regulator is used to power RC servo motor which drives arm.

Figure 20: Pololu D15V70F5S3 Regulator

3.2.5 DC Motor and Encoder

- **HN-GH12-1634T-30:1 DC Motor**

Wheels actuated with presented motor shown in Figure 21. The motors are tested with PWM signal with duty ratio of 0.5 kHz. Angular velocity of DC motor at 12 V is 200 RPM. Specifications of DC motor listed in Table 3

Figure 21: HN-GH12-1634T-30:1 DC motor

Table 3: DC motor Specifications

PARAMETER	SPECIFICATION
Rated Voltage	12 VDC
Rated Load at 12 VDC	0.78 kg-cm
No load Speed at 12 VDC	200RPM ±%10
Speed at Rated Load (0.78 kg-cm)	163 RPM ±%10
No load Current at 12 VDC	<115 mA
Current at Rated Load (0.78 kg-cm)	<285 mA
Gear Ratio	30:1
Shaft Diameter	6 mm

- **US Digital E4P Miniature Optical Encoder**

DC motor angular position measured with presented optical encoder shown in Figure 22 and specifications given in Table 4

Figure 22: US Digital E4P Miniature Optical Encoder

Table 4: Encoder Specifications

PARAMETER	SPECIFICATION
Axial shaft play acceptance	0.020 inch
Cycle per revolution (CPM)	300
Supply voltage	5 V
Supply Current	21 mA
Vibrational Limit (5Hz to 2kHz)	20 G
Rise Time	500 ns

3.2.6 Li-po battery

11.1 V Li-po battery used as power source. Li-po batteries has a wide range of application areas. Most advantage of the Li-Po's is the high density of energy than Ni-Cad and other batteries.

Figure 23: THK 11.1 V Li-Po Battery

3.2.7 Savöx SH-1290MG Servo Motor

Savöx servo motor is one of the powerfull Rc servo on the market. Rc servos has a closed loop feed back inside so user can not obtain any feedback data. It is used by simply appliying PWM signal .In this project 50 Hz PWM signal applied with duty ratio of %5-10 to move arm between ±60°

Figure 24: Savöx SH-1290MG Servo Motor

Table 5: Servo Motor Specifications

PARAMETER	SPECIFICATION
Speed(@4.8 V)	0.06 s/60°
Torque(@4.8 V)	0.4 Nm
Gear	Metal
Bearing	2BB
Weight	56.4 g
Frequency	250-333 Hz

3.3 Single DOF IMU

A test bench is designed to develop an inertial measurement unit. Micro electromechanical system (MEMS) type gyro and accelerometer sensors are placed on a rotating platform. Actual angular position is measured by an encoder. Basically complementary and Kalman filter based estimators are designed and implemented on the test bench. Parameters of the estimators are optimized by using experimental data. Satisfactory results are achieved.

Inertial measurement is essential for most of the robotic systems, unmanned vehicles and many other dynamical systems. Inertial measurement units (IMU) consist of accelerometers, gyros, and the magnetometers as fundamental sensors. Availability MEMS sensors initiated the design of many low cost and small volume IMUs. Fusion of these sensors is essential to reach orientation information, namely roll, pitch and the yaw angles and relevant angular velocities. It consists of an accelerometer and a gyro together with an estimator. A test bench is designed to develop the IMU, shown in Figure 25. MEMS gyro and accelerometer sensors are placed on rotating platform with a cubic base. Actual angular position of the platform is measured by an encoder. In addition, a commercial IMU is also placed on the platform to compare with the developed one.

3.3.1 Test Bench

Figure 25 shows the physical test bench consisting of a DC motor with an encoder, gyro, accelerometer and Microstrain GX2 commercially available IMU. The setup is connected to the computer via Humusoft PCI MF624 Data Acquisition Card. Real time control and data acquisition is performed by Matlab Real Time Windows Target (RTWT) Toolbox.

Position of the platform is controlled by the PID controller. Motor position is received from the encoder. Corresponding angular velocity is derived via numerical derivation. Desired position of the platform is given as a chirp signal to get a rich data for parameter optimization of the estimator. Schematic of the control system is given below in Figure 26. Position and velocity measurement from commercial IMU

are also acquired for comparison. Accelerometer and gyro measurements of the developed IMU are acquired.

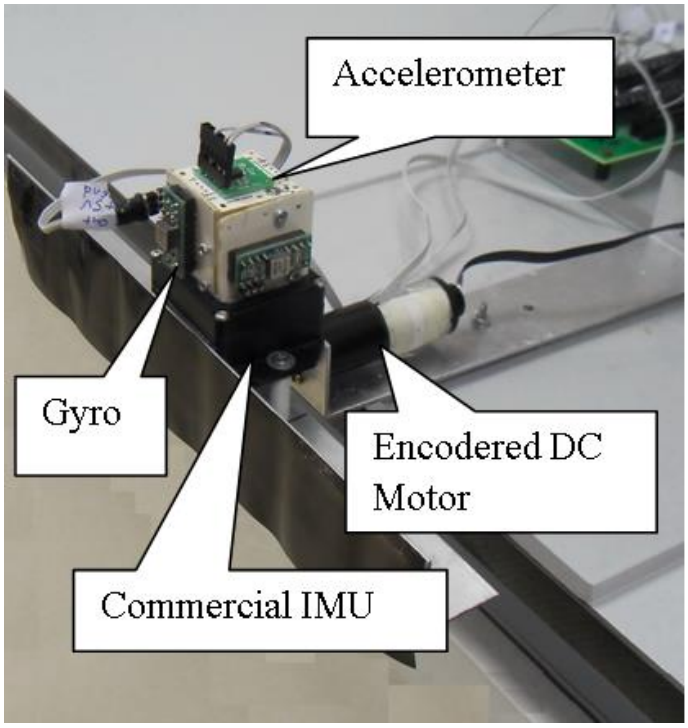

Figure 25: IMU test Bench

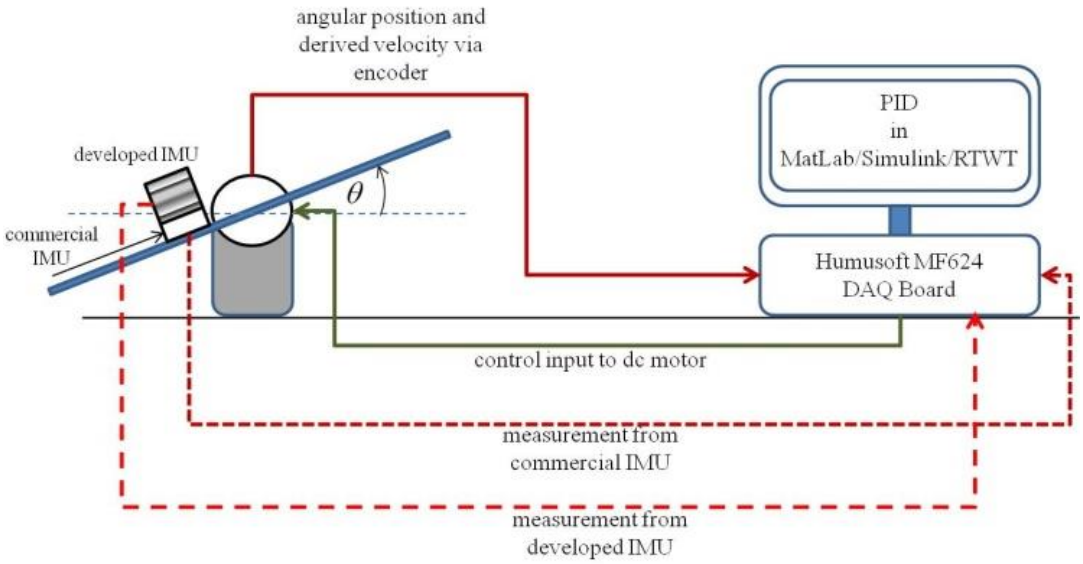

Figure 26: Detailed Schematic of the Test Bench

3.3.2 Estimators

Accelerometers can be used as inclination measurement at low frequencies. Integral of the gyro output can be used to get inclination at high frequencies. Both of the sensor measurements can be fused to estimate the inclination at low and high frequencies. In this study complementary and Kalman filter based estimators are presented.

3.3.3 Complimentary Filter

Basic principle of the complementary filter is to fuse the low pass filtered accelerometer output (calibrated to give inclination angle due to gravitational acceleration) with the high pass filtered inclination angle induced from the integral of the gyro measurement. General structure of the Complementary Filter is shown below in Figure 27.

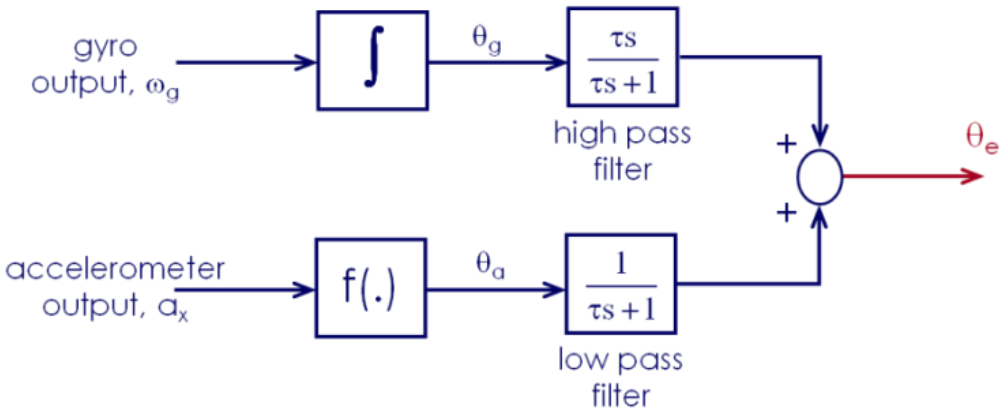

Figure 27: Complimentary Filter Scheme

θ_e is the estimated angular position as the output of the Complementary Filter. τ is the cut-off frequency of the both low pass and high pass filters. Also different cut-off frequencies, τ_{lf} and τ_{hf}, are used for the low-pass and high-pass filters respectively in the study. In addition weighting factors, K_a and K_g, are introduced to the filters. Corresponding low-pass and high-pass filters are given below.

$$Lpf = \frac{K_a}{(\tau_{lf} s)+1} \tag{3.1}$$

$$Hpf = \frac{K_g \tau_{hf} s}{\left(\tau_{hf} s\right)+1} \tag{3.2}$$

Acquired data from accelerometer and gyro is processed offline in Simulink, Figure 4. It is assumed that the actual angular position is acquired from the encoder. Error between the actual and estimated angular positions is calculated for each time point.

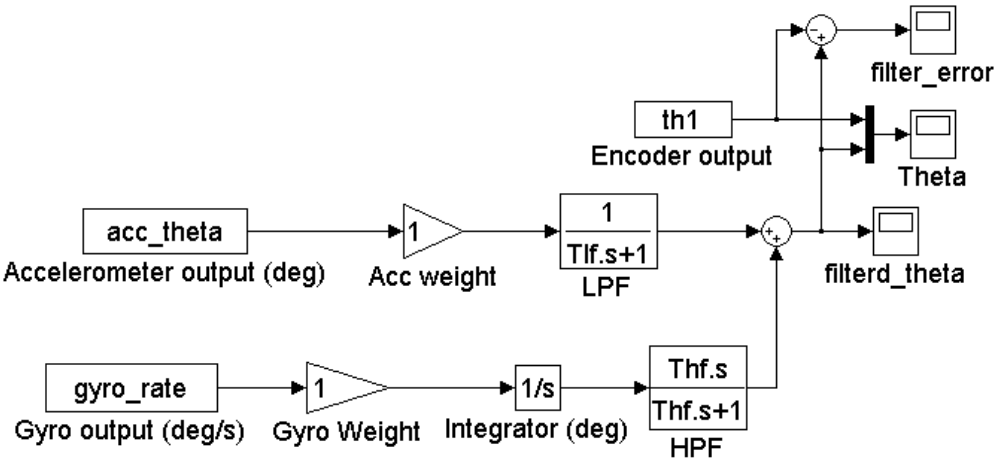

Figure 28: Complementary Filter in Simulink

Cut-off frequencies and weighting factors are the elements of the design vector to minimize the error based cost function. Utilized Complementary Filters within the optimization algorithm are summarized in Table 6.

Table 6: Utilized Variations of CF

K_a	K_g	τ_f	τ_{hf}	**Estimator**
1	1	τ	τ	Standard CF
≠	≠	τ	τ	Weighted CF
1	1	τ_f	τ_{hf}	CF with different cut-off freq.
≠	≠	τ_f	τ_{hf}	Weighted CF with different cut-off freq.

3.3.4 Kalman Filter

Kalman Filter (KF) is the second structure that is utilized to estimate the orientation. In addition, KF also estimates the gyro bias. This improves the accuracy of the angular velocity measurements. Accelerometer and gyro measurements are modeled as follows.

$$\mathbf{x} = \begin{bmatrix} x_1 \\ x_2 \end{bmatrix} = \begin{bmatrix} \theta \\ d_g \end{bmatrix} \tag{3.3}$$

$$\dot{\mathbf{x}} = \begin{bmatrix} \dot{x}_1 \\ \dot{x}_2 \end{bmatrix} = \begin{bmatrix} \dot{\theta} \\ \dot{d}_g \end{bmatrix} = \begin{bmatrix} 0 & -1 \\ 0 & 0 \end{bmatrix} \begin{bmatrix} \theta \\ d_g \end{bmatrix} + \begin{bmatrix} 1 \\ 0 \end{bmatrix} \omega_g + \begin{bmatrix} n_{x1} \\ n_{x2} \end{bmatrix} \tag{3.4}$$

$$\mathbf{y} = \theta_a = \begin{bmatrix} 1 & 0 \end{bmatrix} \begin{bmatrix} \theta \\ d_g \end{bmatrix} + n_a \tag{3.5}$$

$$\mathbf{A} = \begin{bmatrix} 0 & -1 \\ 0 & 0 \end{bmatrix}, \mathbf{B} = \begin{bmatrix} 1 \\ 0 \end{bmatrix}, \mathbf{H} = \begin{bmatrix} 1 & 0 \end{bmatrix} \tag{3.6}$$

θ is the actual angular position desired to be estimated. d_g is the gyro drift or bias. ω_g is the gyro measurement. θ_a is the accelerometer output which is calibrated to give inclination measurement. n_{x1}, n_{x2} and n_a are representing terms for process noise and measurement noise correspondingly. State vector that includes actual angular position and gyro drift are estimated by KF. Well known time update and measurement update equations that construct the KF are given below.

$$\hat{x}_k = \hat{x}_k^- + K_k \left(z_k - H\hat{x}_k^- \right) \tag{3.7}$$

$$P_k^- = AP_{k-1}A^T + Q \tag{3.8}$$

$$K_k = P_k^- H^T \left(H P_k^- H^T + R \right)^{-1} \tag{3.9}$$

$$\hat{x}_k = \hat{x}_k^- + K_k \left(z_k - H\hat{x}_k^- \right) \tag{3.10}$$

$$P_k = \left(I - K_k H \right) P_k^- \tag{3.11}$$

Process and measurement noises are modelled as Gaussian random signals with the following properties.

$$p(n_x) \sim N(0, Q) \tag{3.12}$$

$$p(n_a) \sim N(0, R) \tag{3.13}$$

P is the error covariance matrix. $\hat{x}_k$ is the estimated state vector at time step k. Acquired data from accelerometer and gyro is processed offline in Simulink, Figure 29. As a variation of standard KF, a weighted KF is also utilized. Weighting factors K_g and K_a are multiplied with ω_g and θ_a to scale the contributions of gyro and accelerometer outputs. Elements of Q and R matrices and weighting factors are the elements of the design vector to minimize the error based cost function. Kalman Filters within the optimization algorithm are summarized in Table 7.

Table 7: Utilized Variations of KF

K_a	K_g	Estimator
1	1	Standard KF
≠	≠	Weighted KF

Simulink Model of Kalman Filter

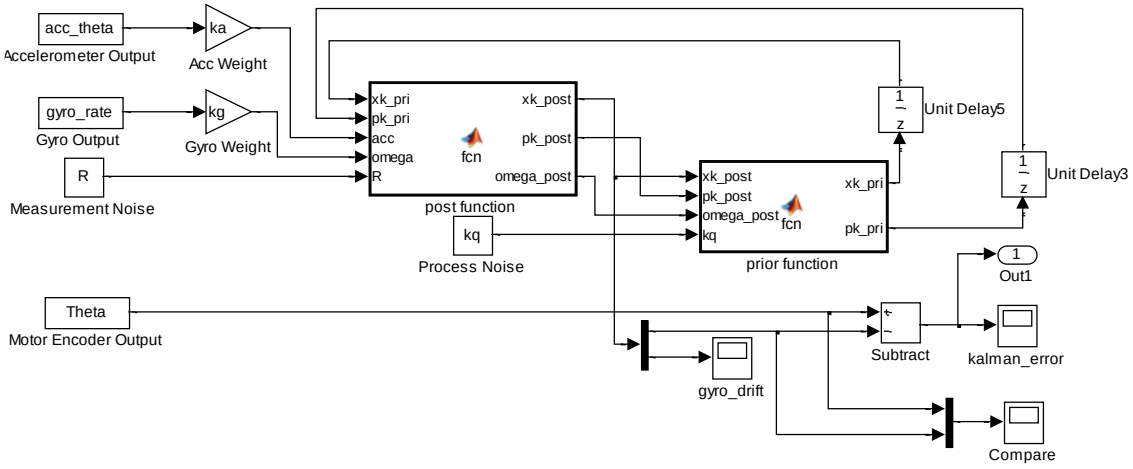

Figure 29: Kalman Filter in Simulink

3.3.5 Optimization of Filter Parameters

Acquired angular position of the platform from encoder together with the accelerometer and gyro outputs are utilized to optimize the filter parameters. They are adjusted to minimize the difference between the actual position and estimated position by Least-Squares Minimization technique. p is the parameter set of the filter. θ_i is the actual angular position and $\hat{\theta}_i$ is the estimated angular position obtained from the filter at i'th data point. $\hat{p}$ is the optimal parameter set that minimizes the cost function below.

$$\hat{p} = \min_{p} \left[\frac{1}{N} \sum_{i=1}^{N} \left(\theta_i - \hat{\theta}_i(p) \right)^2 \right] \tag{3.14}$$

Actual angular position of the platform is given below in Figure 30.

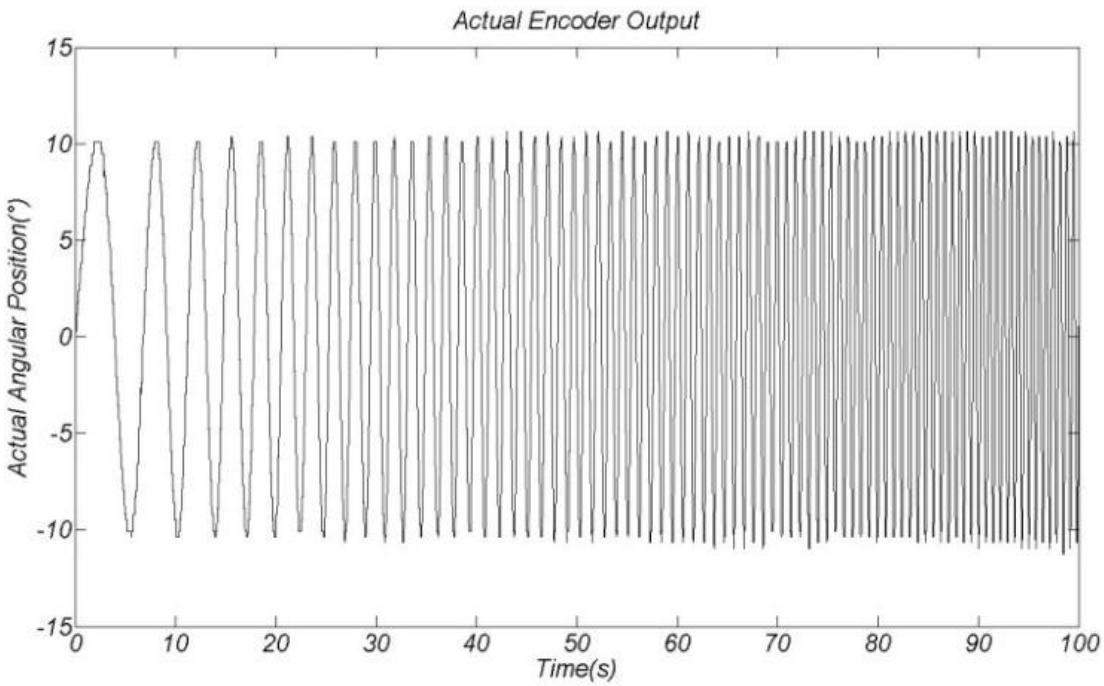

Figure 30: Actual Angular Position

Calibrated accelerometer output is presented in Figure 31.

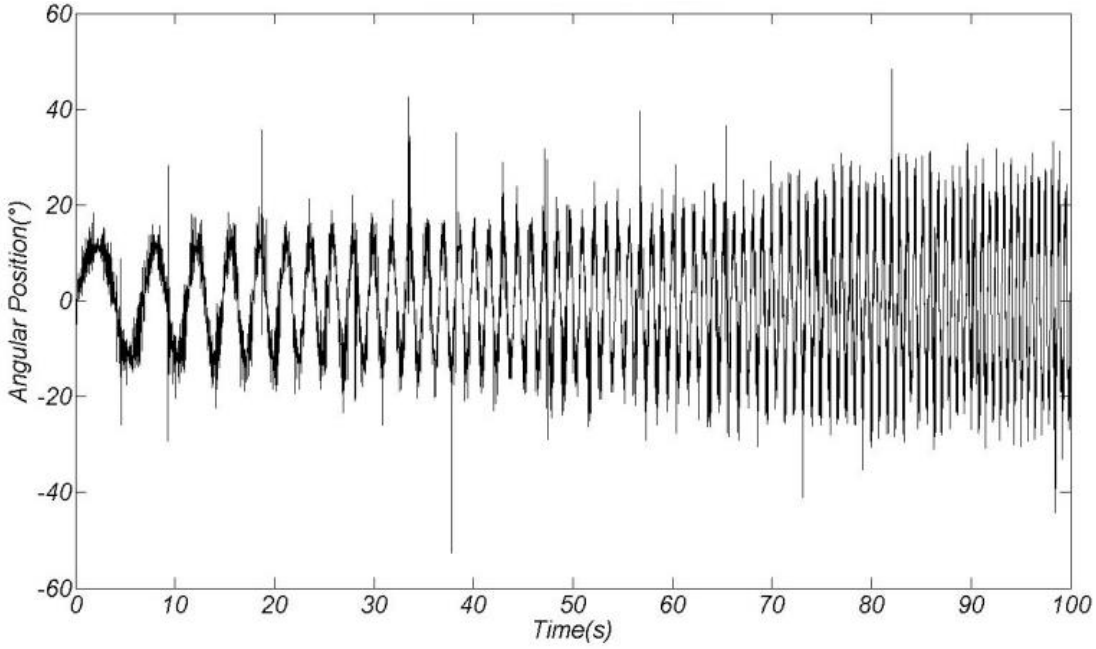

Figure 31: Accelerometer Measurement

Angular velocity measurement from gyro is given in Figure 32.

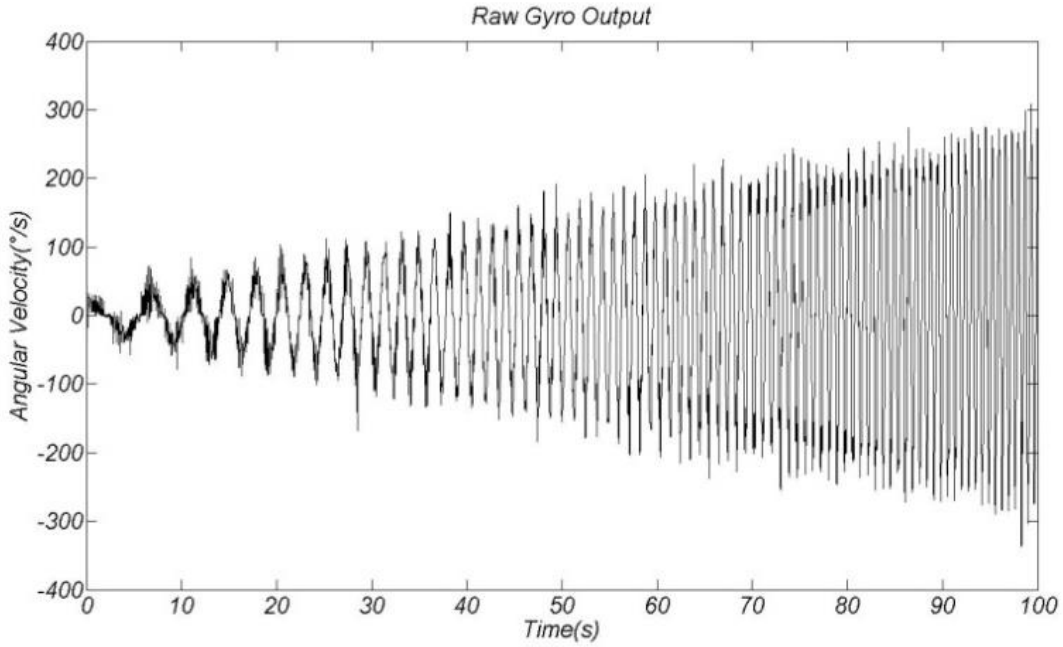

Figure 32: Gyro Measurement

Using the actual position and the sensor data standard CF is optimized. Figure 33 reveals the actual and optimized CF estimations.

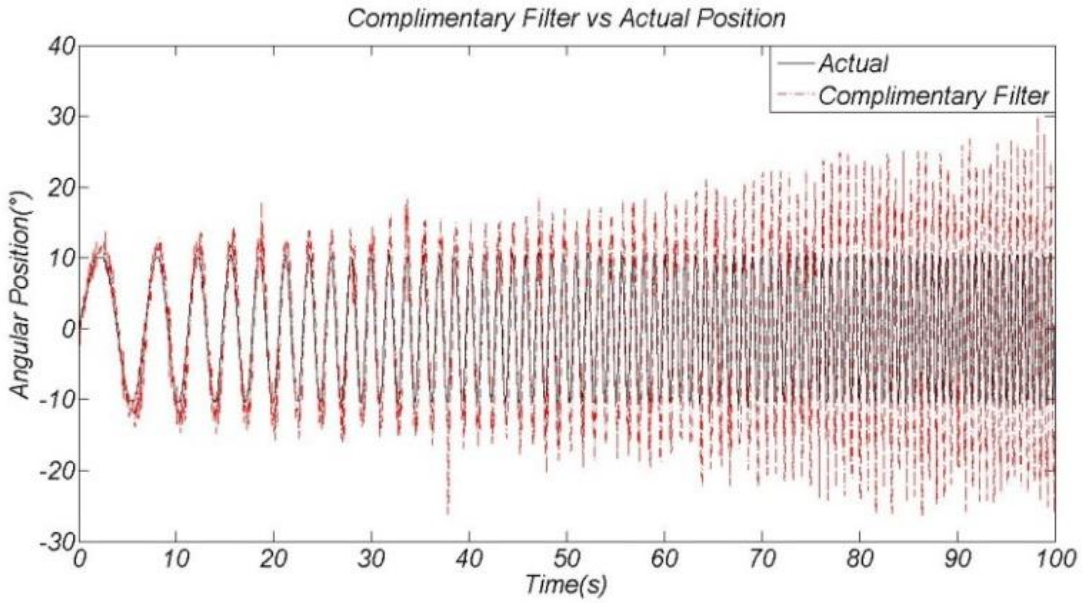

Figure 33: Actual Position and Standard CF Estimation

Figure 34 shows the estimated angular position from CF with different low-pass and high-pass cut-off frequencies.

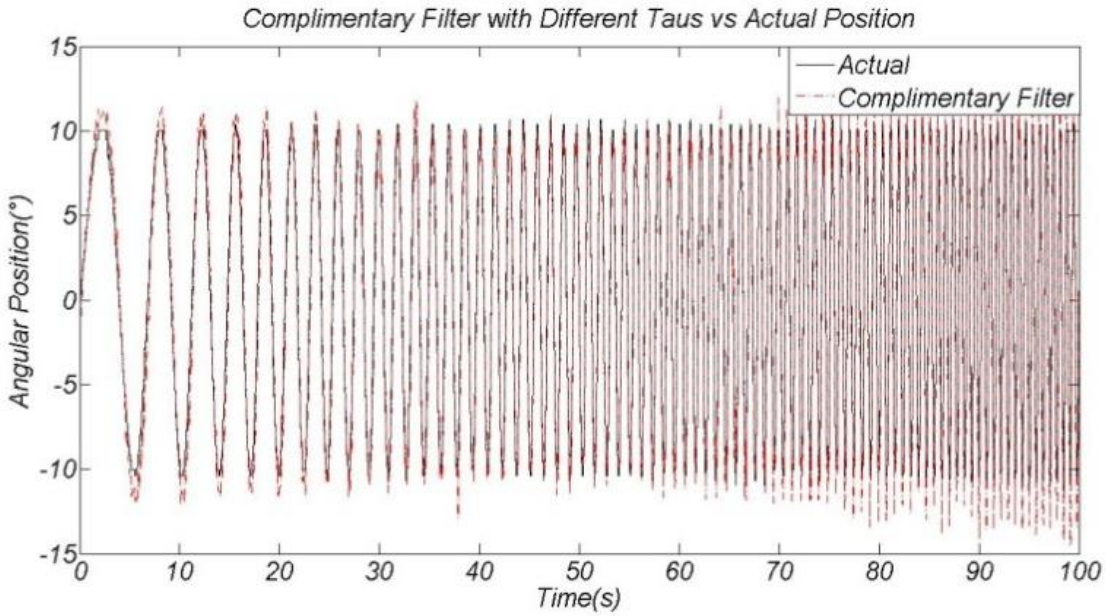

Figure 34: Actual Position and Estimation of CF with Different Cut-off Frequencies

Figure 35 shows the estimated angular position from weighted CF.

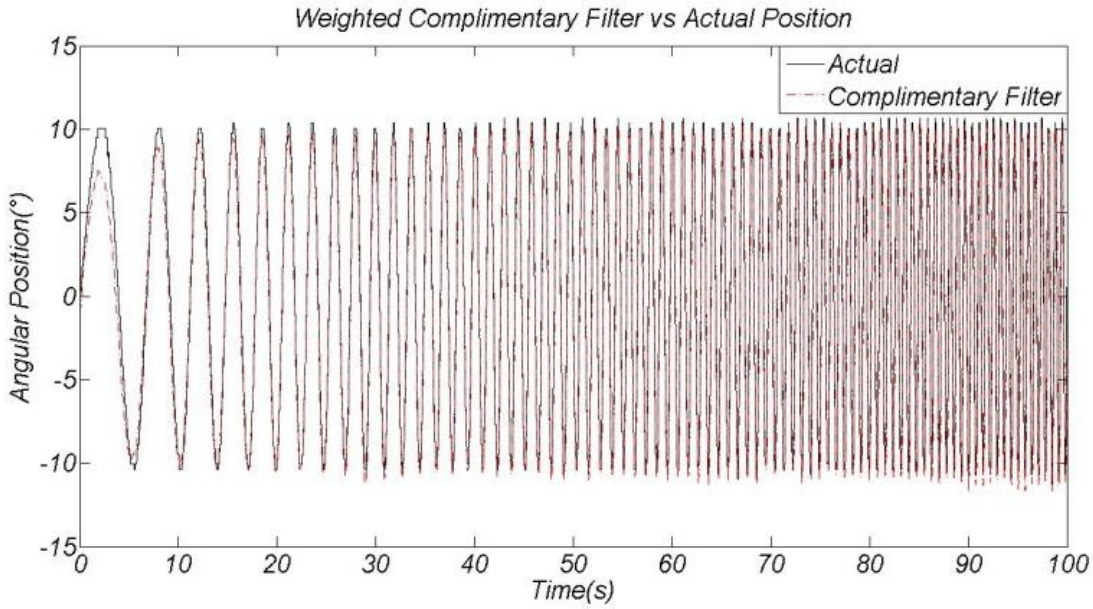

Figure 35: Actual Position and Estimation of Weighted CF

Final plot for CF is Figure 36 for the weighted CF with different cut-off frequencies.

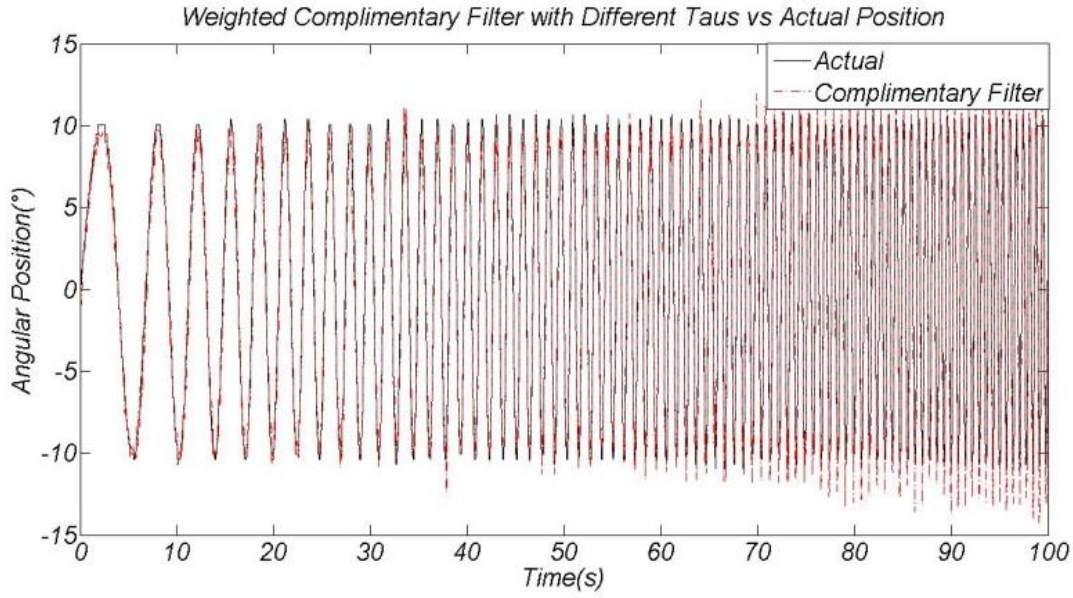

Figure 36: Actual Position and Estimation of Weighted CF with Different Cut-off Frequencies

Figure 37 shows the estimation from the standard KF.

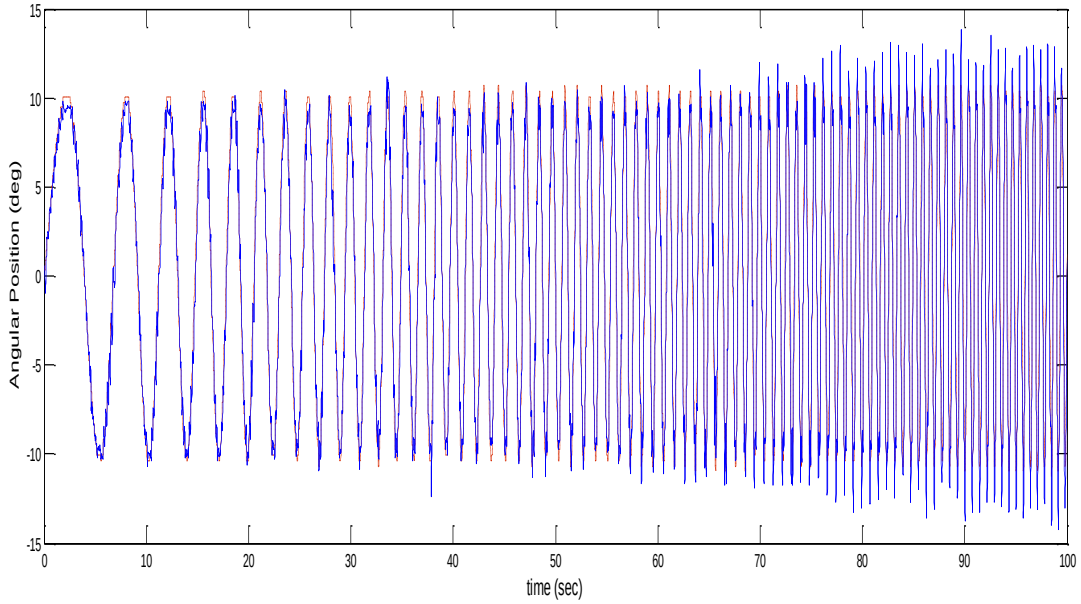

Figure 37: Actual Position and Estimation of Standard KF

Finally Figure 38 shows the response of weighted KF.

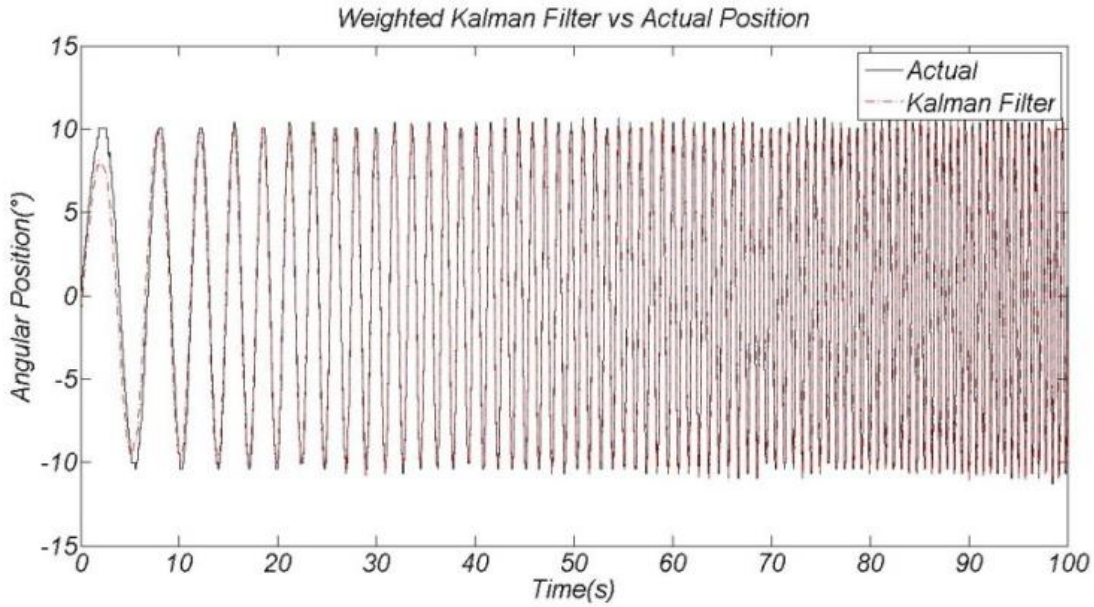

Figure 38: Actual Position and Estimation of Weighted KF

It is seen that CF and KF has better performances at different frequencies. Therefore, we have fused the CF and KF estimations in a similar way as it is done in standard

CF. Output of the CF is high-pass filtered and output of standard KF is low-pass filtered and they are summed up. The result is given below in Figure 39.

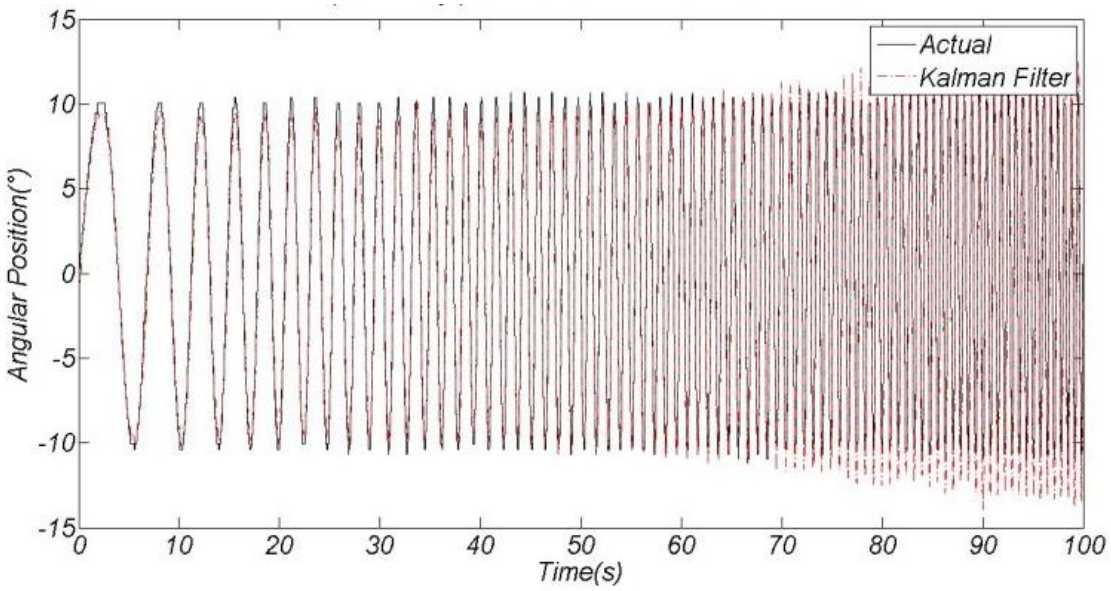

Figure 39: Actual Position and Estimation of fused CF and KF

CHAPTER 4

MATHEMATICAL MODELLING

Dynamical model of the system derived with Lagrange-Euler method using the FBD (free body diagram) in Figure 40.

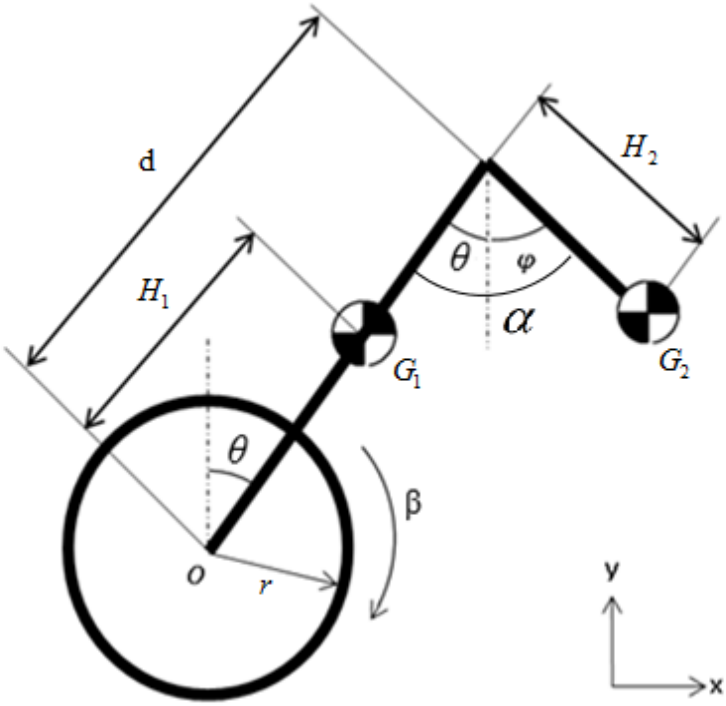

Figure 40: FBD of the System

Linear displacement of the center of mass of the body in x and y directions given in below equations.

$$x_b = x + H_1 sin\theta \tag{4.1}$$

$$y_b = H_1 cos\theta \tag{4.2}$$

Derivatives of the displacements gives the linear velocity.

$$\dot{x}_b = \dot{x} + H_1\dot{\theta}cos\theta \tag{4.3}$$

$$\dot{y}_b = -H_1\dot{\theta}sin\theta \tag{4.4}$$

Linear displacement of the center of mass of the arms in x and y directions given in below

$$x_a = x + dsin\theta + H_2\sin(\alpha - \theta) \tag{4.5}$$

$$y_a = dcos\theta - H_2\cos(\alpha - \theta) \tag{4.6}$$

$$\dot{x}_a = \dot{x} + d\dot{\theta}cos\theta + H_2(\dot{\alpha} - \dot{\theta})\cos(\alpha - \theta) \tag{4.7}$$

$$\dot{y}_a = -d\dot{\theta}sin\theta + H_2(\dot{\alpha} - \dot{\theta})\sin(\alpha - \theta) \tag{4.8}$$

Lagrange Equations

$$\frac{d}{dt}\left(\frac{\partial L}{\partial \dot{q}_i}\right) - \frac{\partial L}{\partial q_i} + \frac{\partial D}{\partial q_i} = F_i \tag{4.9}$$

Generalized coordinates q_1, q_2, q_3 respectively β, θ, α given below

$$\begin{aligned} q_1 &\to \beta = \frac{x}{r} & F_1 &\to T_1 \\ q_2 &\to \theta & F_2 &\to 0 \\ q_3 &\to \alpha & F_3 &\to T_2 \end{aligned} \tag{4.5}$$

$$K = M_w(\dot{\beta}r) + \frac{1}{2}M_b(\dot{x}_2^{\,2} + \dot{y}_2^{\,2}) + \frac{1}{2}Ma(\dot{x}_3^{\,2} + \dot{y}_3^{\,2}) + \frac{1}{2}J_a(\dot{\alpha} - \dot{\theta})^2 + \frac{1}{2}J_b\dot{\theta}^2 + J_w\dot{\beta}^2 \tag{4.6}$$

$$P = -M_a g\left((dcos\theta) - H_2\cos(\alpha - \theta)\right) - M_b g H_1 cos\theta \tag{4.7}$$

$$D = b_0\dot{x}^2 + b_1(\dot{\beta} - \dot{\theta})^2 + \frac{1}{2}b_2(\dot{\alpha} - \dot{\theta}) \tag{4.8}$$

Lagrange functions L in equation 13 given below

$$L = K - P \tag{4.9}$$

$$L = M_w\left(\dot{\beta}r\right) + \frac{1}{2}M_b\left(\dot{x}_2{}^2 + \dot{y}_2{}^2\right) + \frac{1}{2}Ma\left(\dot{x}_3{}^2 + \dot{y}_3{}^2\right) + \frac{1}{2}J_a(\dot{\alpha} - \dot{\theta})^2 + \frac{1}{2}J_b\dot{\theta}^2 + J_w\dot{\beta}^2 - M_a g\left(\left(d\cos\theta\right) - H_2\cos\left(\alpha - \theta\right)\right) - M_b g H_1 \cos\theta \tag{4.10}$$

DC motor mathematical model expressed as in Figure 41

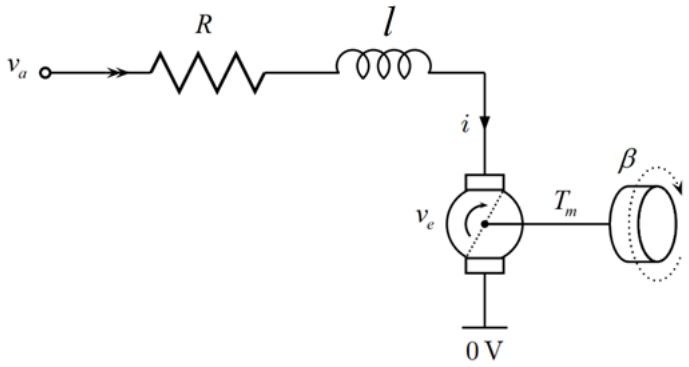

Figure 41: DC motor model

Motor torque expressed as $\mathrm{T} = \mathrm{f}(\mathrm{V})$ .Relation between Armature current and voltage expressed as

$$T_m = K_t i \tag{4.11}$$

$$V_a - Ri - l\frac{di}{dt} - V_e = 0 \tag{4.12}$$

Back electromotor force (EMF), $\mathrm{V_e}$ expressed

$$V_e = K_e\dot{\beta}_m \tag{4.13}$$

l assumed as very small and eliminated, so

$$i = \frac{V - K_e\dot{\beta}_m}{R} \tag{4.14}$$

Equations rearranged and expressed in

$$T_m = K_t\left(\frac{V}{R} - \frac{K_e}{R}\dot{\beta}_m\right) \tag{4.15}$$

$\dot{\beta}_m$ is the angular speed of the motor shaft. It can be written in terms of rotation of wheel and pitch angle of body as

$$\beta_m = n\beta - \theta \tag{4.16}$$

$$\dot{\beta}_m = n\dot{\beta} - \dot{\theta} \tag{4.17}$$

Motor torque in Equation 4.11 can be expressed in terms of wheel torque as below.

$$T_w = nT_m \tag{4.18}$$

If equations rearranged it can be written as

$$T_w = \frac{nVK_t}{R} - \frac{nK_tK_e}{R}(n\dot{\beta} - \dot{\theta}) \tag{4.19}$$

Physical parameters of the system given in Table 8.

Table 8: Parameters of the System

M_a	Mass of arm [kg]	0.04
M_w	Mass of wheel [kg]	0.127
M_b	Mass of body [kg]	1.26
J_a	Moment of inertia of arm [kgm^2]	0.0016
J_b	Moment of inertia of body [kgm^2]	0.129
J_w	Moment of inertia of wheel [kgm^2]	0.0007
g	Gravitational acceleration [m/s^2]	9.81
H_1	Distance between wheel center and COM of body [m]	0.22
H_2	Distance between joint of arm to COM of arm [m]	0.2
d	Length of body [m]	0.56
r	Wheel Radius [m]	0.1
n	Gear ratio	30
R	Terminal resistance of DC motor (Ω)	8.7
Kt	Torque Constant	0.1429
Ke	Back EMF constant	0.1429
b_0	Friction between wheel and ground	0.05
b_1	Friction between body and wheel	0.005
b_2	Friction between body and arm	0.01

4.1 State Space Representation

Dynamic equation of this model obtained using Euler-Lagrange equation as

$$\mathbf{T} = \mathbf{M}(q)\ddot{q} + \mathbf{H}(q,\dot{q})\dot{q} + \mathbf{g}(q) \tag{4.20}$$

where $\mathbf{q} = [q_1, q_2, q_3]^T \in R^3$, $\mathbf{T} = [T_1, 0, T_2] \in R^3$ are vector of generalized coordinates and input torque vector for the mobile inverted pendulum platform, $\mathbf{M} \in R^3, \mathbf{H} \in R^3$, $\mathbf{g(q)} \in R^3$ are respectively inertia, centrifugal and coriolis, and gravitational matrices.

Linearizing equations around equilibrium point $[\beta, \theta, \alpha, \dot{\beta}, \dot{\theta}, \dot{\alpha}] = [0,0,0,0,0,0]$, state equations will be calculated below:

$$\begin{aligned} \dot{\mathbf{x}}(t) &= \mathbf{A}\mathbf{x}(t) + \mathbf{B}\mathbf{u}(t) \\ \mathbf{y} &= \mathbf{C}\mathbf{x}(t) \end{aligned} \tag{4.21}$$

After substituting the values as in Table 8, state space model of system without arm is obtained in Equation 4.22. and Equation 4.23

$$A = \begin{bmatrix} 0 & 0 & 1 & 0 \\ 0 & 0 & 0 & 1 \\ 0 & -89.56 & 210.1 & -6.59 \\ 0 & 42.65 & -64.1 & 2.02 \end{bmatrix}, \quad B = \begin{bmatrix} 0 \\ 0 \\ -49.11 \\ 14.98 \end{bmatrix} \tag{4.22}$$

$$C = \begin{bmatrix} 1 & 0 & 0 & 0 \end{bmatrix}, \; D = 0 \tag{4.23}$$

Controllability of the system without arm can be checked considering the rank of the following controllability matrix.

$$Co = \begin{bmatrix} B & BA & BA^2 & \ldots & BA^{n-1} \end{bmatrix} \tag{4.24}$$

The rank of the controllability matrix is calculated by Matlab software and the controllability matrix becomes,

$$Rank\begin{bmatrix} B & BA & BA^2 & BA^3 \end{bmatrix} = 4 \tag{4.25}$$

State space model of the system with arm is obtain in Equation 4.26 and Equation 4.27.

$$A=\begin{bmatrix} 0 & 0 & 0 & 1 & 0 & 0 \\ 0 & 0 & 0 & 0 & 1 & 0 \\ 0 & 0 & 0 & 0 & 0 & 1 \\ 0 & -79.94 & -0.59 & 176.31 & -5.12 & -0.08 \\ 0 & 40.06 & 0.95 & -55.25 & 1.53 & 0.12 \\ 0 & 28.49 & -24.76 & -21.98 & 3.79 & -3.15 \end{bmatrix},\quad B=\begin{bmatrix} 0 & 0 \\ 0 & 0 \\ 0 & 0 \\ -41.31 & -9.25 \\ 12.94 & 0.60 \\ 5.15 & 158.32 \end{bmatrix} \tag{4.26}$$

$$C=\begin{bmatrix} 1 & 0 & 0 & 0 & 0 & 0 \end{bmatrix},\ D=0 \tag{4.27}$$

Controllability matrix of the system with arm resulted in Equation 4.28.

$$Rank\begin{bmatrix} B & BA & BA^2 & BA^3 & BA^4 & BA^5 \end{bmatrix}=6 \tag{4.28}$$

As a result both system with arm and without arm is completely state controllable.

CHAPTER 5

CONTROLLER DESIGN AND SIMULATIONS

The dynamics of n-link robotic manipulators are usually modelled by n coupled second-order nonlinear differential equations. Robotic manipulator models contain uncertain elements, which are not known exactly. Therefore, the dynamics of robotic manipulators are generally classified as uncertain dynamic system, and can be described by ordinary differential equation where the bound of uncertainty is known The controller considered for the robotic manipulators need to move payloads of different masses from one point to another with good balance of the stability and response Furthermore, it is important to design a single controller which work for a range of payload mass instead of design a series controllers or changing control parameters for each equilibrium points on-line. We present a controller based on coefficient diagram method CDM to achieve desired performance specifications. The construction of this controller is based on coefficient diagram method. For historical development, basic properties of this control structure and more references see Coefficient diagram method is an algebraic approach applied to polynomial loop in the parameter space, where a special diagram called coefficient diagram is used as the vehicle to carry the necessary information, and as the criteria of good design. The simplicity of the controller structure made it very powerful for systems with uncertainties.

Coefficient diagram method may be classified in algebraic approach that expressed with polynomial form. Also it may be considered between conventional and modern control theories. The controllers and controller parameters designed by conventional methods usually are based on trial-and-error procedure that, in general, will not yield optimal solution. The modern control methods have also same physical limitations, although they achieve predefined desired closed loop performances. In CDM; the performance specification, stability index, x, and equivalent time constant τ, are specified in the closed loop transfer function and

related to the controller parameters algebraically in explicit form. The controller is first assumed in the simplest possible form to satisfy the basic specification, and gradually improved to meet full specifications. The simultaneous design nature exists in CDM, gives advantages to designer to keep good balance between the rigor of the requirements and the complexity of the controller. The advantages of CDM have been discussed in Here first the fundamental principles of CDM are illustrated by considering the closed-loop characteristic equation and the standard form of CDM and their results are summarized.

5.1 CDM Concept

In CDM, the controllers are designed based on the stability index known as γ_i and equivalent time constant known as τ which are synthesized from the characteristic polynomial of the closed-loop transfer function in Equation 5.1.

$$P(s) = a_n s^n + a_{n-1} s^{n-1} + ... + a_1 s + a_0 \tag{5.1}$$

The choice of stability index γ_i due to the control design specifications must satisfy the following inequality

$$\gamma_i > 1.5\gamma_i^* \tag{5.2}$$

where γ_i is the stability limit and is defined as

$$\gamma_i^* = \frac{1}{\gamma_{i+1}} + \frac{1}{\gamma_{i-1}}; \tag{5.3}$$

From the characteristic polynomial $P(s)$ given in Equation 5.1, the stability index γ_i and equivalent time constant τ are respectively described in general term as in Equation 5.4 and 5.5

$$\gamma_i = \frac{a_i^2}{a_{i-1}a_{i+1}}, \qquad (i = 1,2,...,n-1) \tag{5.4}$$

$$\tau = \frac{a_1}{a_0} \tag{5.5}$$

where γ_i is the stability index and τ is the equivalent time constant.

$$\tau = \frac{t_s}{2.5} \sim \frac{t_s}{3} \tag{5.6}$$

$$\gamma_0, \gamma_n = \infty \tag{5.7}$$

In general the stability index is recommended as

$$\gamma_{n\text{-}1} = ... = \gamma_3 = y_2 = 2, \ \gamma_1 = 2.5 \tag{5.8}$$

known as standard stability index.

Finally the characteristic polynomial known as the desired characteristic polynomial can be expressed as

$$P_m(s) = \frac{\prod_{j=1}^{n-1} \gamma_{n-j}^{j}}{\tau^n} \left[\left\{ \sum_{i=2}^{n} \left(\prod_{j=1}^{i-1} \frac{1}{\gamma_{i-j}^{j}} \right) (\tau s)^i \right\} + \tau s + 1 \right] \tag{5.9}$$
$$= s^n + a_{n-1} s^{n-1} + ... + a_1 s + a_0$$

where $a_{n,} a_{n-1}, ..., a_0$ are the coefficients of the desired characteristic polynomial.

5.2 Controller Design

System state space representation of both arm affecting and without arm affecting models derived. In this section, an Integrator is augmented to the system Equation 4.21 in order to reject the steady-state-error at the arm angle. Since the pendulum angle θ will be naturally kept around zero degree, only linear displacement x used for augmented system without arm is used and for the with arm affecting model linear displacement and arm angle used for augmentation. Thus, the output matrix for system without arm is reduced to

$$H = [1 \quad 0 \quad 0 \quad 0] \tag{5.10}$$

And, the output matrix for the system with arm is reduced to

$$H = \begin{bmatrix} 1 & 0 & 0 & 0 & 0 & 0 \\ 0 & 0 & 1 & 0 & 0 & 0 \end{bmatrix} \tag{5.11}$$

The block diagram of the linearized augmented system is illustrated in Figure 42.

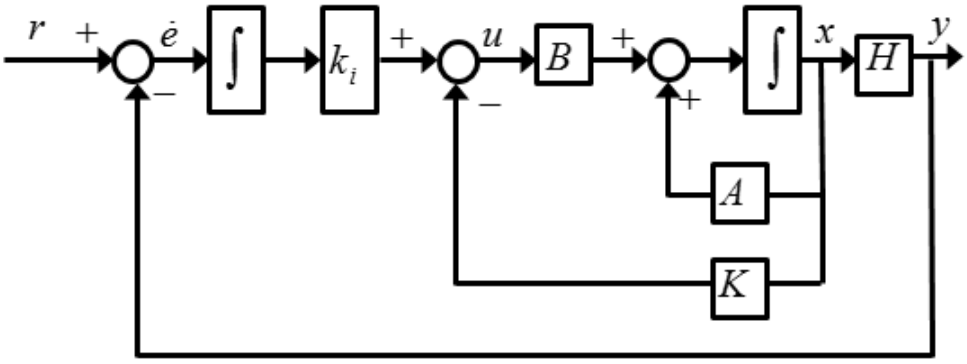

Figure 42: Block Diagram of Augmented System

The control law u(t) assigned as in Equation 5.12.

$$\mathbf{u}(t) = \text{-}\mathbf{K}\mathbf{x}(t) \tag{5.12}$$

Thus, the state equation and output equation of the augmented system shown in Equation 5.13

$$\begin{aligned} \dot{\mathbf{x}}_\mathbf{a}(t) &= \mathbf{A}_\mathbf{a}\mathbf{x}_\mathbf{a}(t) + \mathbf{B}_\mathbf{a}\mathbf{u}(t) + \mathbf{F}\mathbf{r}(t) \\ \mathbf{y}(t) &= \mathbf{H}_\mathbf{a}\mathbf{x}_\mathbf{a}(t) \end{aligned} \tag{5.13}$$

Where $\mathbf{y}(t)$ is the control output and $\mathbf{r}(t)$ is the reference signal.

$$A_a = \begin{bmatrix} A & 0 \\ -H & 0 \end{bmatrix}, B_a = \begin{bmatrix} B \\ 0 \end{bmatrix}, H_a = \begin{bmatrix} H & 0 \end{bmatrix}, F = \begin{bmatrix} 0 \\ 1 \end{bmatrix} \tag{5.14}$$

$$x_a = \begin{bmatrix} x(t) \\ e(t) \end{bmatrix} \tag{5.15}$$

In pair of A and B of Equation 4.21 is controllable and $\begin{bmatrix} A & 0 \\ -H & 0 \end{bmatrix}$ is full rank, then the system in Equation 5.13 becomes completely state controllable. Therefore, the control law $\mathbf{u}(t)$ can be assigned as given by

$$\mathbf{u}(t) = -\mathbf{K}_a\mathbf{x}_a(t) = -\begin{bmatrix}\mathbf{K} & -ki\end{bmatrix}\mathbf{x}_a(t) \tag{5.16}$$

Where $\mathbf{K}$ and ki are state feedback gains and integral gain respectively. Therefore, the closed-loop system of the augmented system 5.13 with the control law is

$$\dot{\mathbf{x}}_a(t) = (\mathbf{A}_a - \mathbf{B}_a\mathbf{K}_a)\mathbf{x}_a(t) + \mathbf{F}\mathbf{r}(t) \tag{5.17}$$

The main idea of CDM is to choosing the coefficients of the characteristic equations. To do this desired coefficients of the desired characteristic equations are used. It is known that to place the desired poles in to the desired location pole placement method can be used. Notice that the eigenvalues of $\mathbf{A}_a$ do not depend on $\mathbf{K}_a$. Thus, if the system is not completely state controllable, then there are eigenvalues of matrix $\mathbf{A}_a$ that cannot be arbitrarily placed. Therefore, to place the eigenvalues of matrix $\mathbf{A}_a - \mathbf{B}_a\mathbf{K}_a$ arbitrarily, the system must be completely state controllable (necessary condition). Next we shall prove a sufficient condition: that is, if the system is completely state controllable, then all eigenvalues of matrix A can be arbitrarily placed.

We prove that rank of the $\mathbf{A}_a$ for both system given in Table 9 is full rank the systems are completely state controllable.

Table 9: Rank of the $\mathbf{A}_a$

System		**Rank**
Without arm	Rank(A_a)=	4
With arm		6

To find the coefficients of the desired equation parameters in Table 10 is used.

Table 10: Parameters of the CDM

System	t_s	γ_i
Without arm	4	$[2.5 \quad 2 \quad 2 \quad 2]$
With arm	4	$[1.5 \quad 1.5 \quad 1.5 \quad 1.5 \quad 1.5 \quad 1.5 \quad 1.5]$

Thus the poles of the systems or Eigen values of $\mathbf{A_a - B_a K_a}$ obtained in Table 11 by using Equation 5.2 to 5.7 and Table 10.

Table 11: Poles of the both system

System	**Poles of desired equation / Eigen values of $\mathbf{A_a - B_a K_a}$**
Without arm	-4.8341 -3.3940 + 1.9821i -3.3940 - 1.9821i -1.0639 + 1.2250i -1.0639 - 1.2250i
With arm	-21385 -134.72 -9.0053 -1.7314 -0.16575 + 1.5787i -0.16575 - 1.5787i -0.93875 + 1.4538i -0.93875 - 1.4538i

Finally $\mathbf{K_a}$ values of augmented system given in Table 12.

Table 12: $\mathbf{K_a}$ *Values*

System	$\mathbf{K_a}$
Without arm	$\begin{bmatrix} 0.2 & 4.45 & -4.13 & 1.06 & -0.14 \end{bmatrix}$
With arm	$\begin{bmatrix} 602.46 & 10904 & 530.24 & 404.85 & 2074.7 & 131.57 & -726.48 & -35.01 \\ 54.77 & 991.76 & 49.83 & 37.22 & 188.57 & 12.88 & -65.96 & -5.97 \end{bmatrix}$

5.3 Simulations

The system is simulated in two different conditions given in Equation 4.22, 4.23, 4.26 and 4.27. In simulations different types of references (square, sine) implemented and stability and tracking performance observed.

5.3.1 First Condition: Arm is not Affecting to Disturbance Rejection

In the first condition arm has no effect on disturbance rejection i.e. state space representation used in Equation 4.22 and 4.23. There is no disturbance affecting on the system as shown in Figure 43. 0.1 Hz sinusoidal reference is applied.

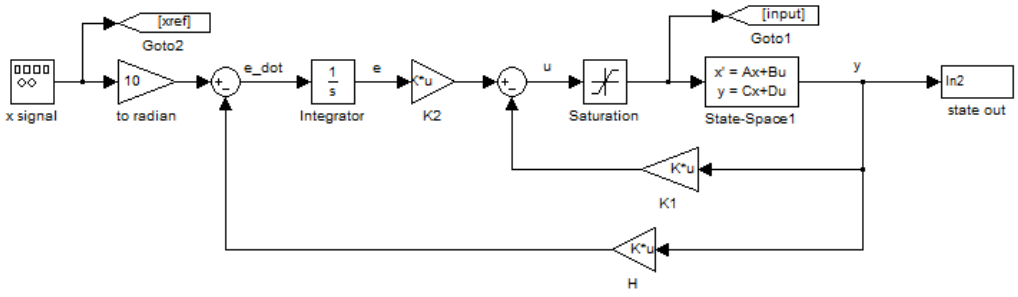

Figure 43: Simulink view of condition with no disturbance exists

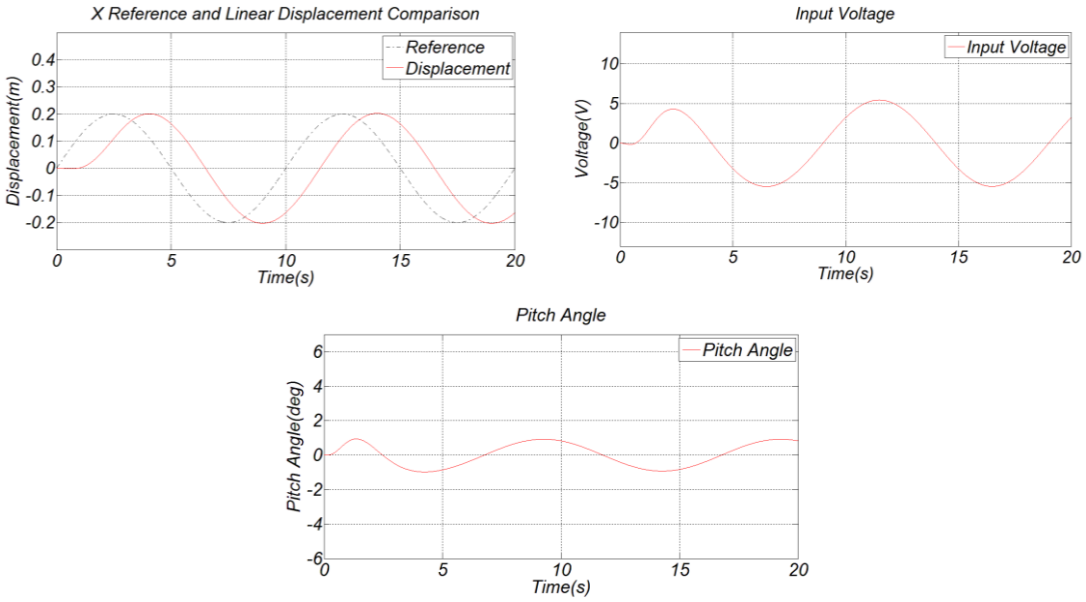

Figure 44: Sinusoidal reference, input voltage, pitch angle with no disturbance results

In Figure 44 it is clearly seen that tracking capability of CDM with given sinusoidal reference is very well. Input voltage is not exceeding the limitations. Body angle is seen making smooth movements.

And also In Figure 45 square type of reference applied. Tracking capability is not good as sinusoidal reference. Input voltage is again in limits. And body angle is not exceeding the point that CDM controller can not stabilize again.

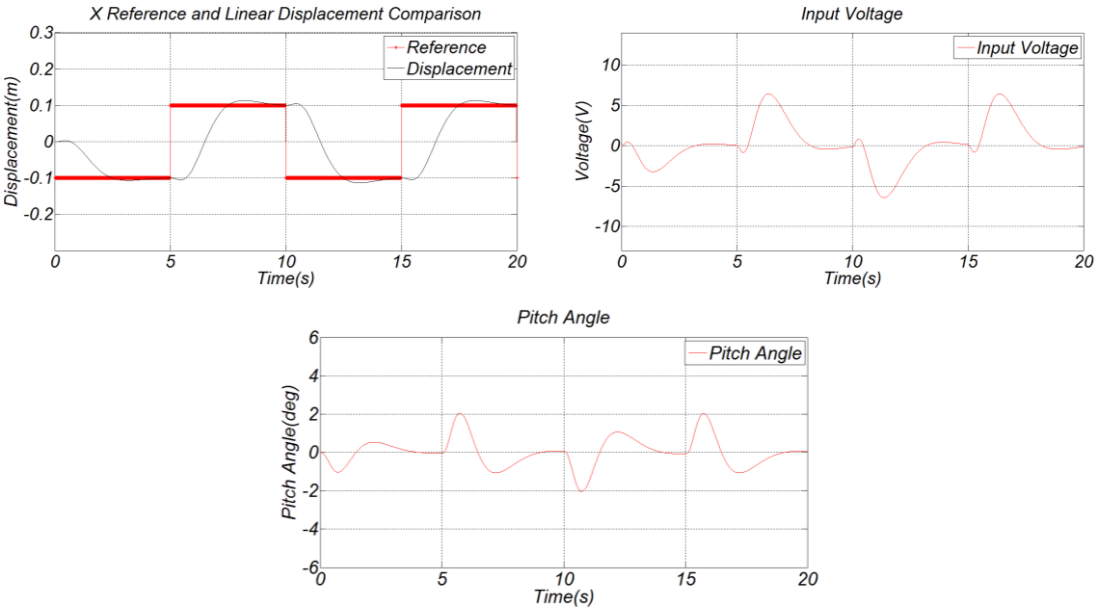

Figure 45: Square reference, input voltage, pitch angle with no disturbance results

There is simulink view of disturbance affecting on the system shown in Figure 46. In this situation arm is not going to help balancing but there will be disturbance applied to the system. Tracking and disturbance rejection capabilities will be observed.

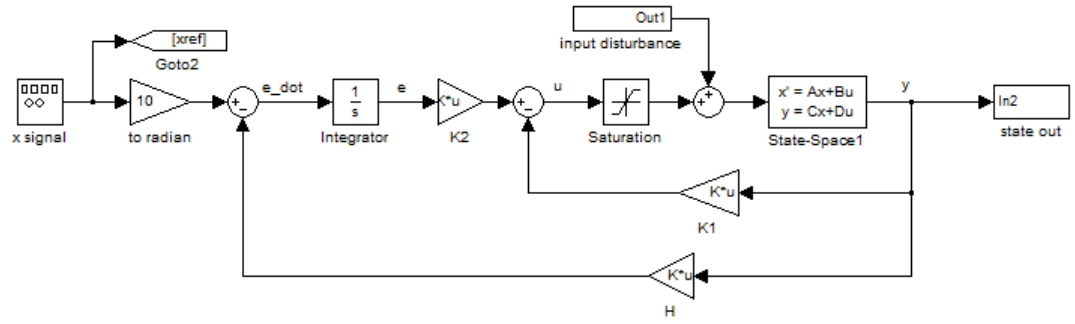

Figure 46: Simulink view of condition with disturbance exists

As we can see in Figure 47 at the time when the disturbance applied there are some movements that has a bad effect on tracking. Input voltage is nearly at the limits. And body angle is moving more than previous experiment.

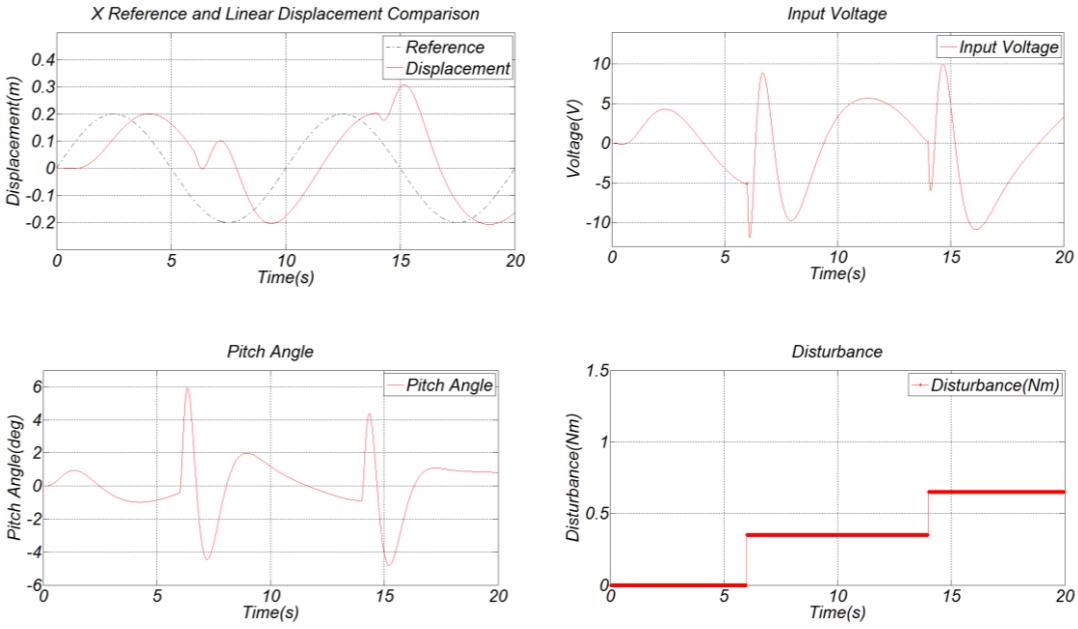

Figure 47: Sinusoidal reference, input voltage, pitch angle and disturbance

Also Disturbance applied the model with square type of reference. There is also bad movements when the disturbance applied.

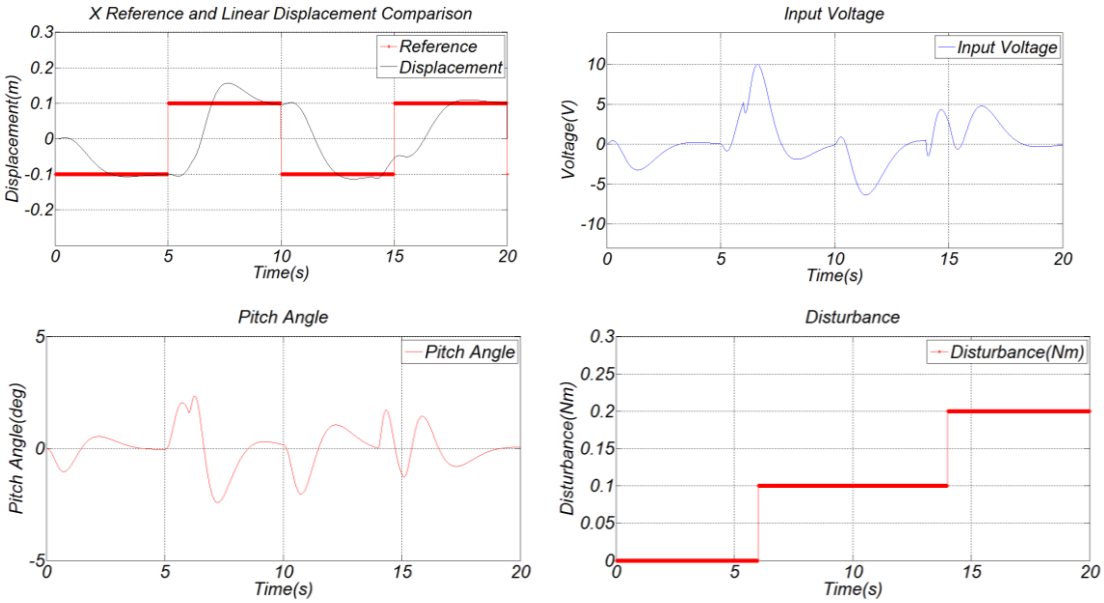

Figure 48: Square reference, input voltage, pitch angle and disturbance

5.3.2 Second Condition: Arm is Affecting to Disturbance Rejection

In the second condition arm has an effect on disturbance rejection i.e. state space representation used in Equation 4.26 and 4.27. There is no disturbance affecting on the system as shown in Figure 49. 0.1 Hz sinusoidal reference is applied.

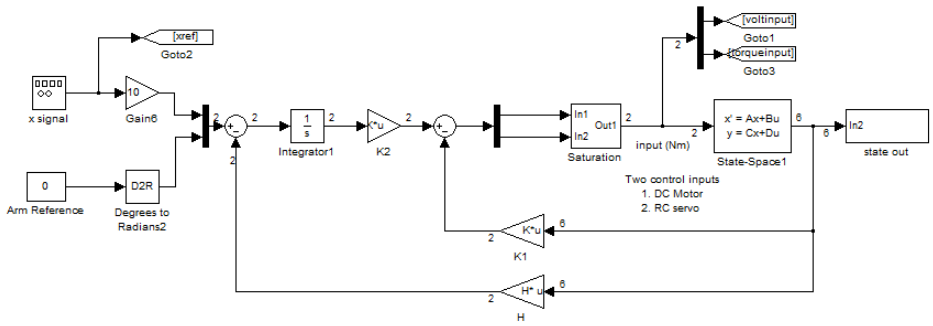

Figure 49: Simulink view of condition with arm and there is no disturbance exists

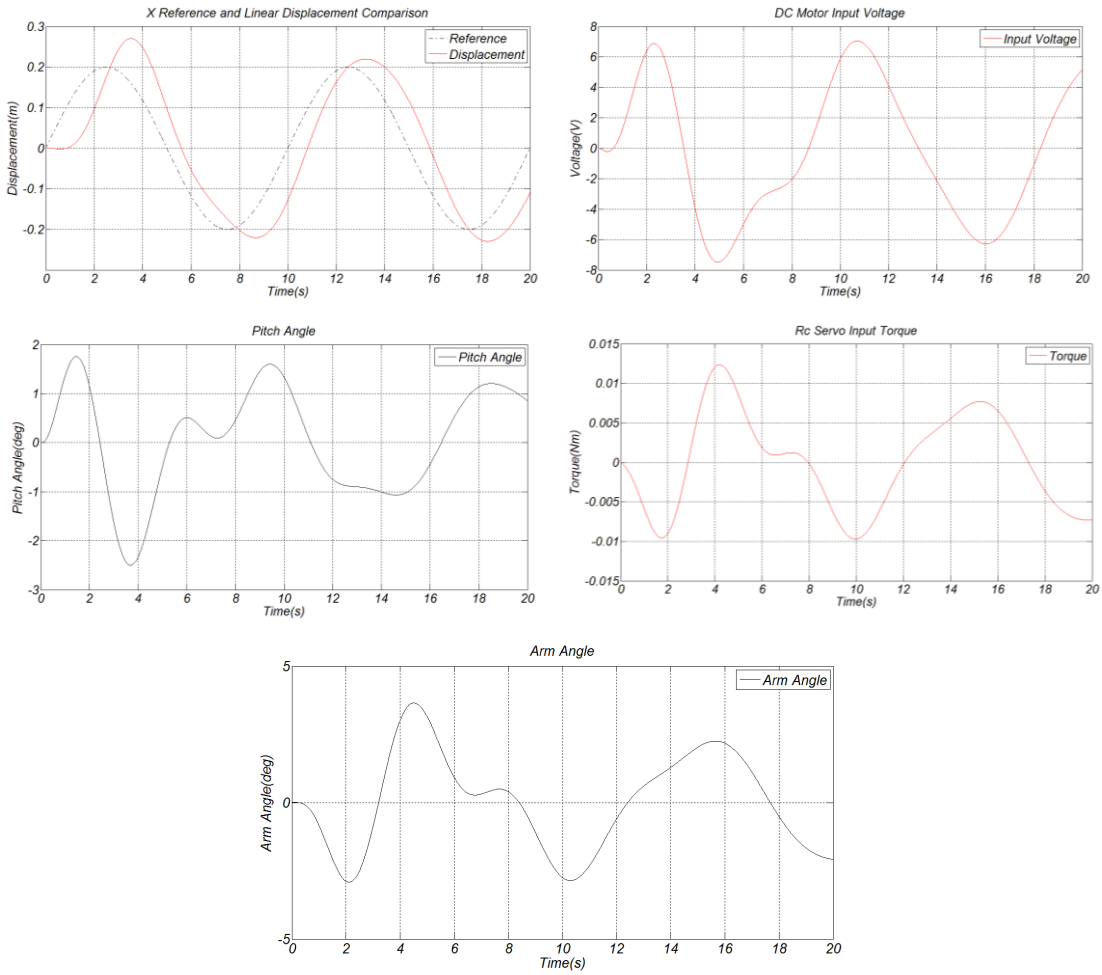

Figure 50: Sinusoidal reference, DC motor input voltage, Rc servo input torque pitch angle, arm angle with there is no disturbance exists

0. 05 Hz square reference is applied in Figure 51.

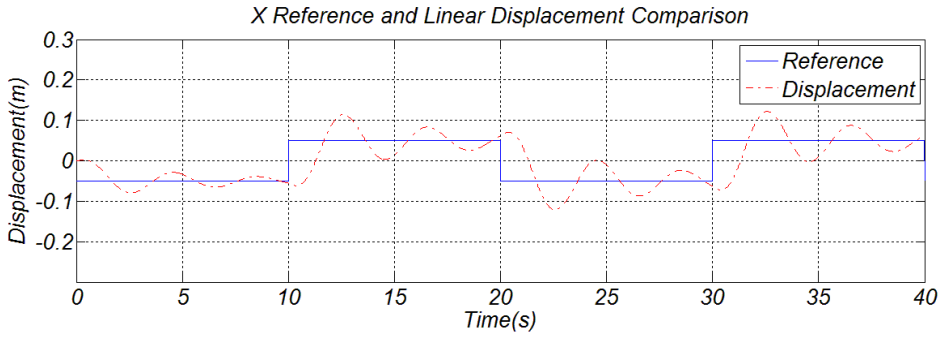

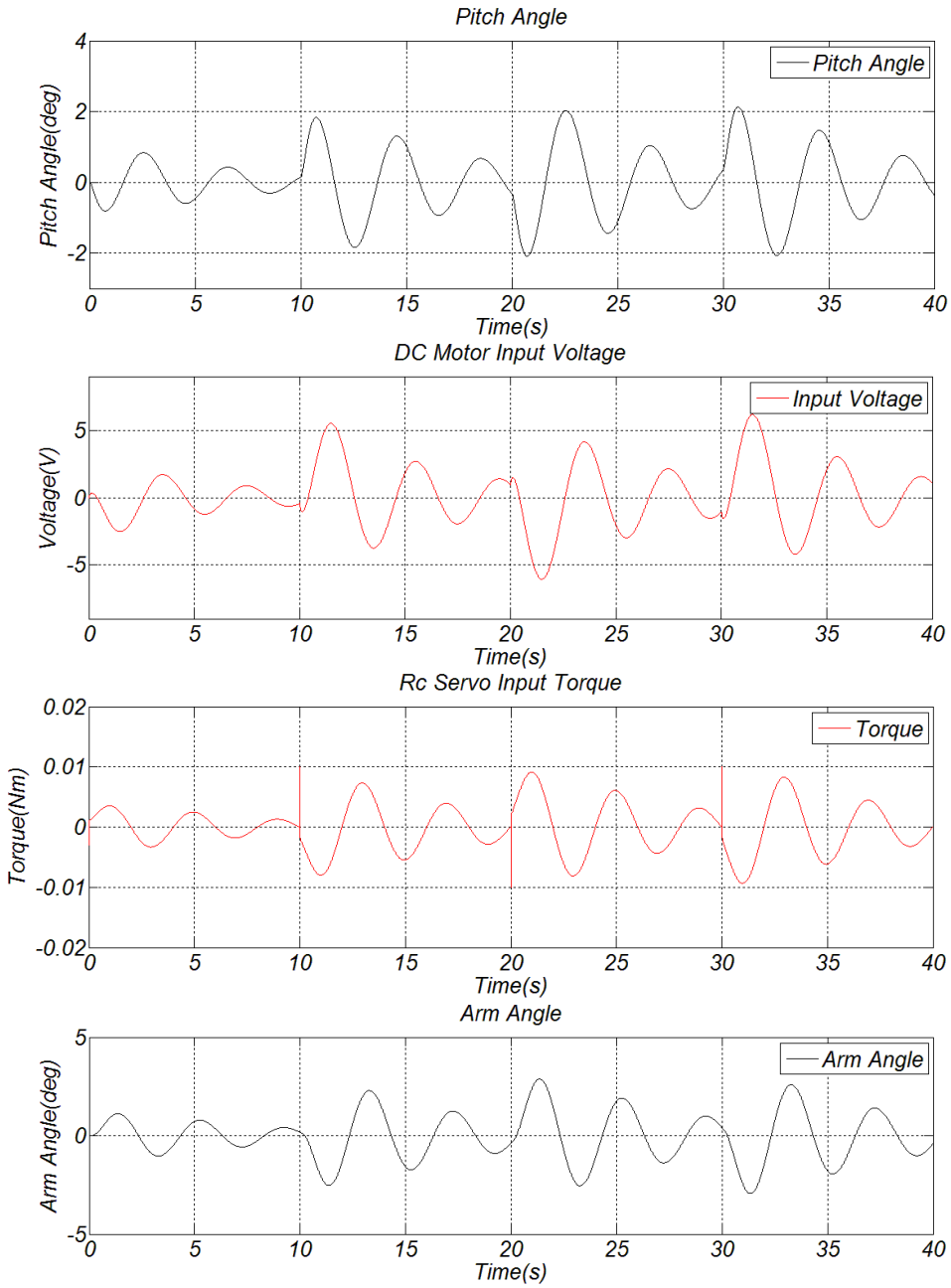

Figure 51: Square reference, DC motor input voltage, Rc servo input torque pitch angle, arm angle with there is no disturbance exists

In Figure 52 disturbance is applied with sinusoidal and square references.

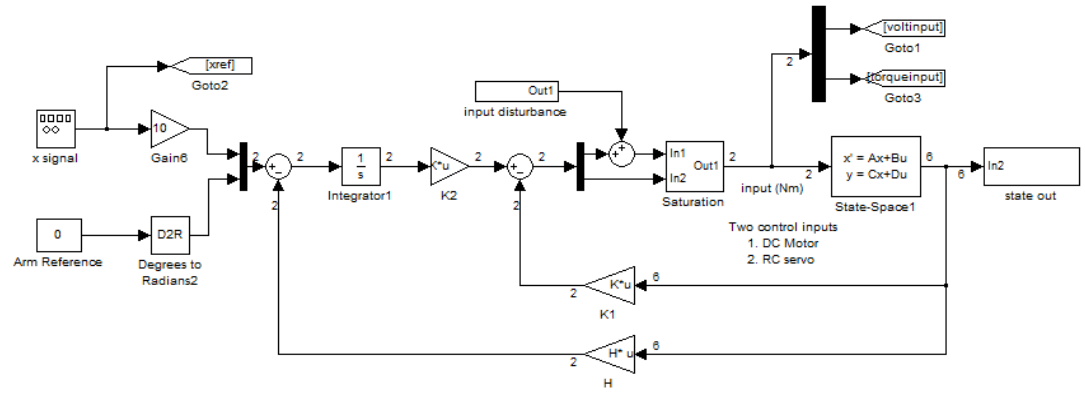

Figure 52: Simulink view of condition with arm and there is disturbance exists

0.1 Hz sinusoidal reference is applied with disturbance in Figure 53

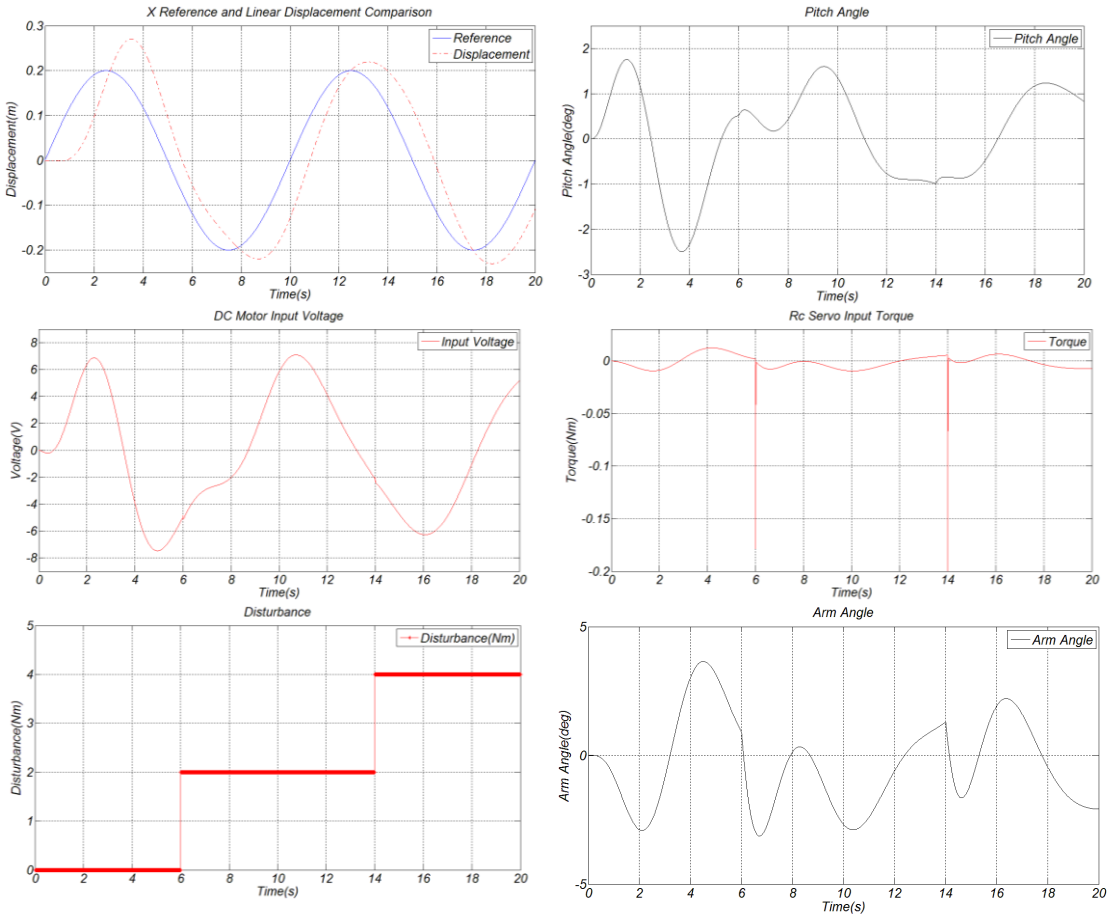

Figure 53: Sinusoidal reference, DC motor input voltage, Rc servo input torque, pitch angle, arm angle and disturbance

0.05 Hz square reference and disturbance is applied and results shown in Figure 54.

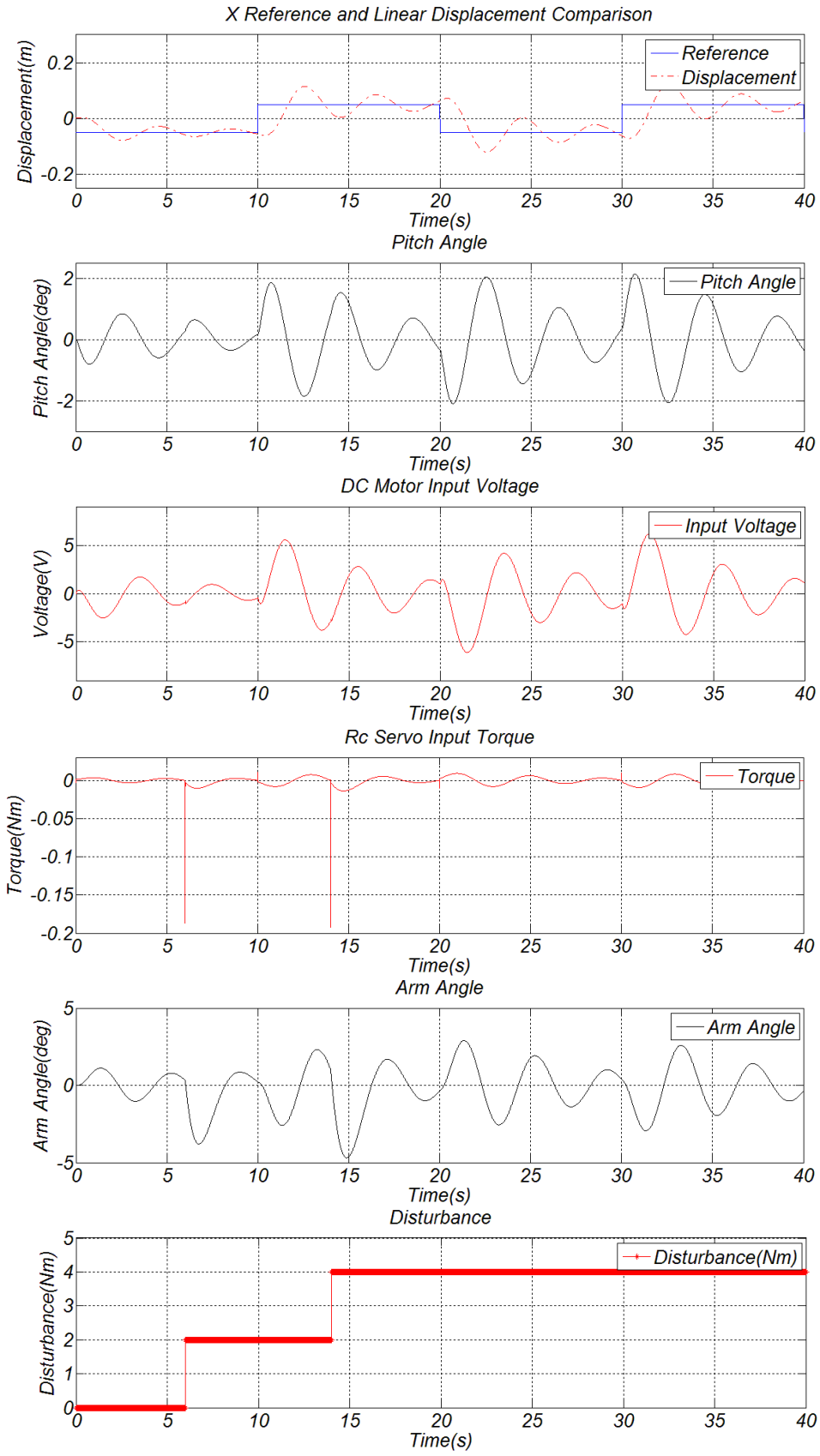

Figure 54: Sinusoidal reference, DC motor input voltage, Rc servo input torque, pitch angle, arm angle and disturbance

In Figure 53 we can see the tracking capability is very good while there is an disturbance effect. Arms is acting well on eliminating disturbances. In Figure 54 we see square type of reference tracking is not well while disturbance rejection capability still good.

To understand well about disturbance rejection and tracking capability of condition with arm and without arm is to compare them in Figure 55, Figure 56, Figure 57, Figure 58.

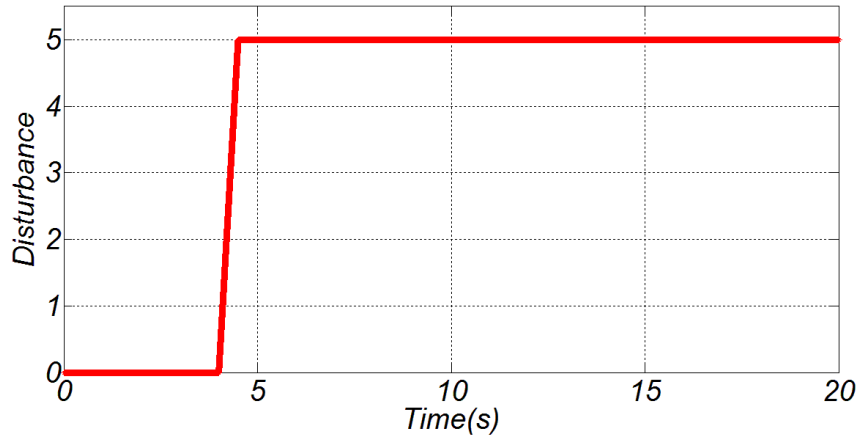

Figure 55: Disturbance Applied to system

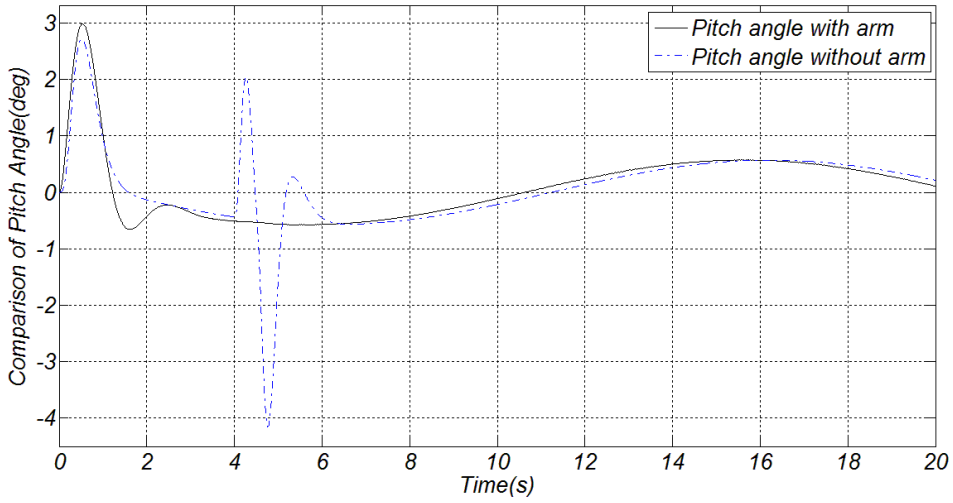

Figure 56: Comparison of body pitch angle

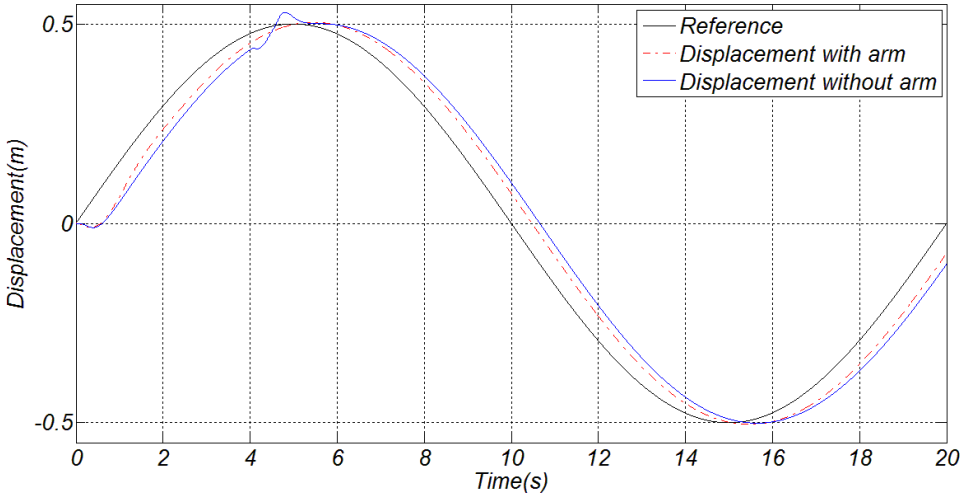

Figure 57: Comparison of linear position

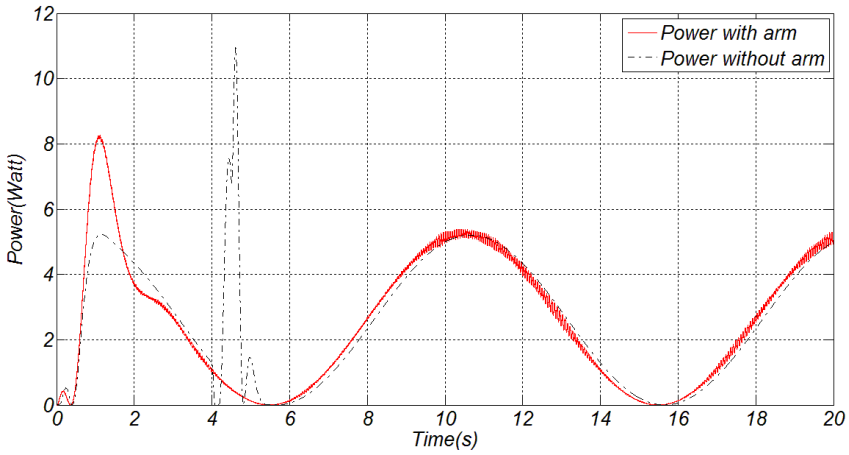

Figure 58: Comparison of power

CDM control in sinusoidal type of reference is giving perfect result while in tracking and eliminating disturbances.

CHAPTER 6

REAL TIME EXPERIMENTS

Real time data obtained by using Xbee RF transmitter/receiver. Arms used as disturbance source and stability performance of CDM controller observed. CDM controller rejects external and arm disturbances while controls the pitch stability and linear displacement.

In CDM controller polynomial coefficients selection is essential. Eigen values of the controller determines the stability characteristic of the system. If Observability and Controllability matrix rank is non zero system is full state controllable hence the system can be controlled with CDM method. The results show us controller can handle stability with different type of reference input.

In real time experiments Standart Manabe form is used and performances observed. $\gamma_{n-1} = \ldots = \gamma_3 = y_2 = 2,\ \gamma_1 = 2.5$ chosen as a Standart Manabe Form with settling time $t_s = 2.3$. In Equation 6.1 Feedback gain vector K_a and in Equation 6.2 poles of the desired characteristic equation is given.

$$\begin{bmatrix} 1.7985 & 14.3980 & -3.4165 & 3.6980 & -2.1552 \end{bmatrix} \tag{6.1}$$

$$\begin{bmatrix} -8.4071 \\ -5.9027 + 3.4471i \\ -5.9027 - 3.4471i \\ -1.8503 + 2.1305i \\ -1.8503 - 2.1305i \end{bmatrix} \tag{6.2}$$

6.1 Controller Software

Matlab Simulink and blockset for DSPIC microcontroller used. Blockset are developed by Lubin Kerheul. Demo blockset allow the user to use 7 pins. Blockset is shown in Figure 59.

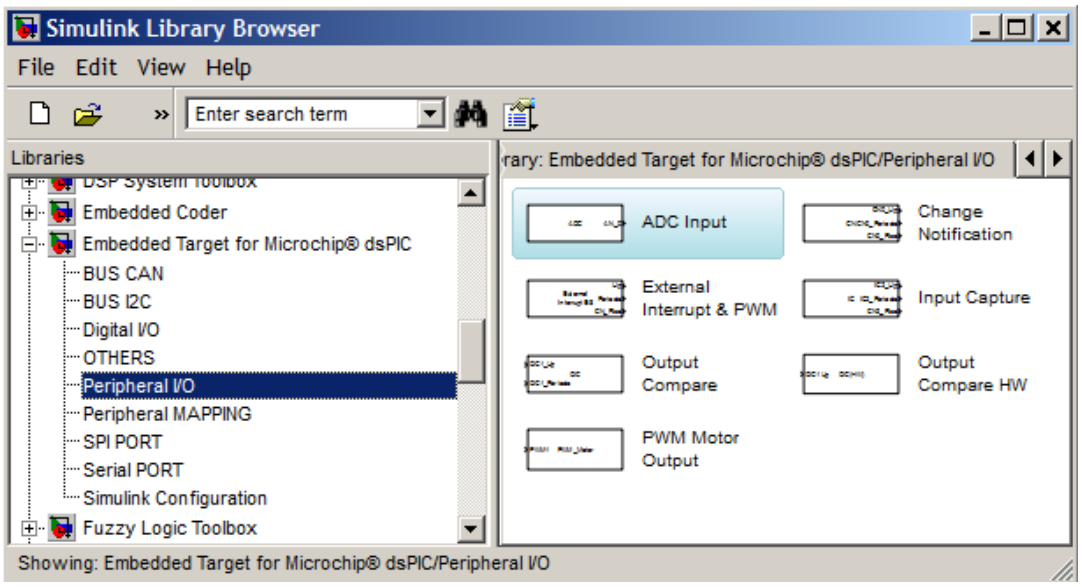

Figure 59: DsPic Blockset for Matlab Simulink

Simulink scheme of CDM Contoller shown in Figure 60.

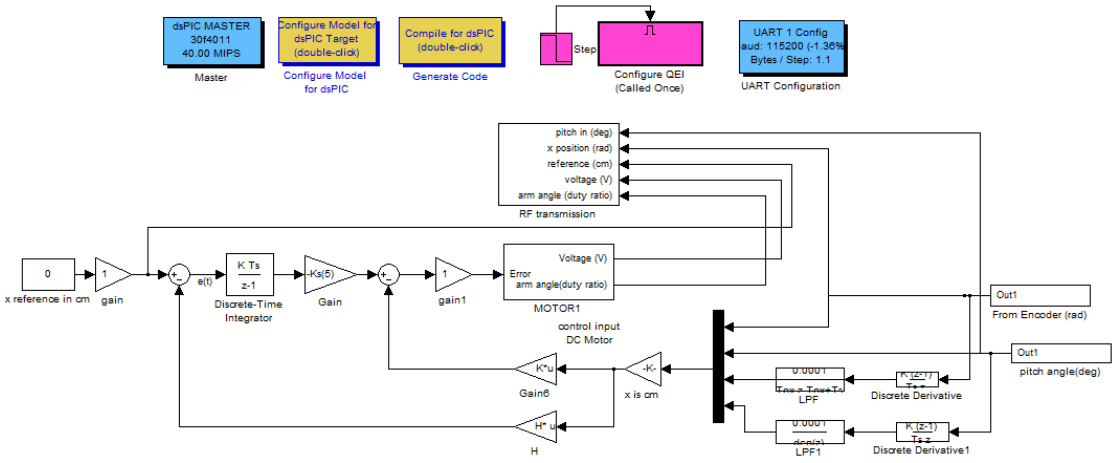

Figure 60: Simulink scheme of CDM Contoller

6.2 Real Time Experiments Without Disturbance

In this subsection real time experiments without disturbance observed.

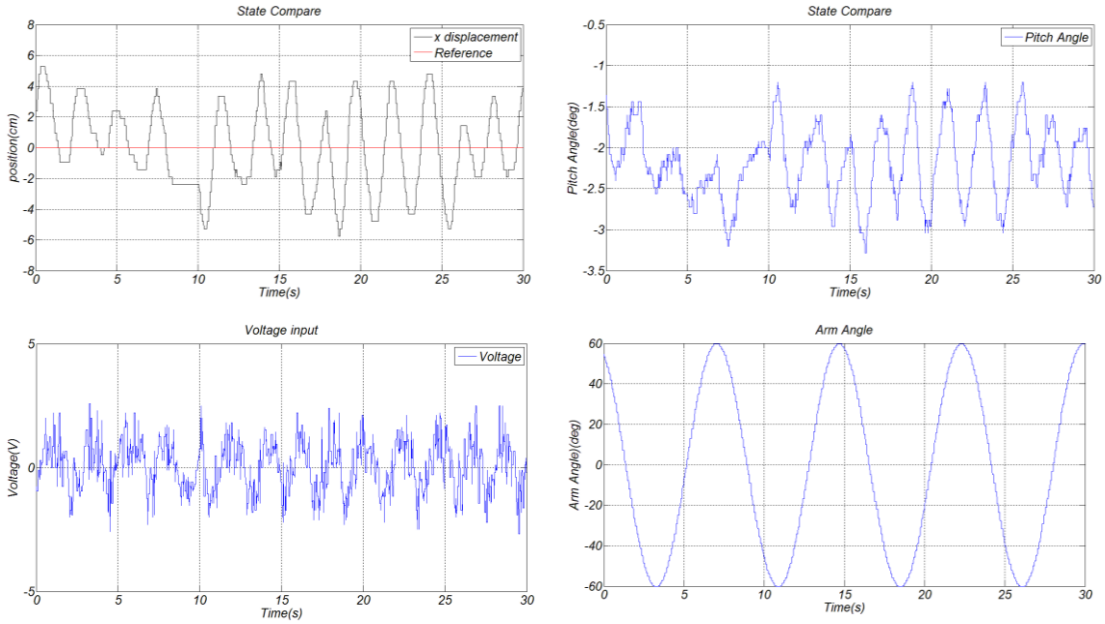

Figure 61: Zero reference without arm disturbance in real time

As seen in Figure 61 tracking capality is very well. Voltage input is under the limits.

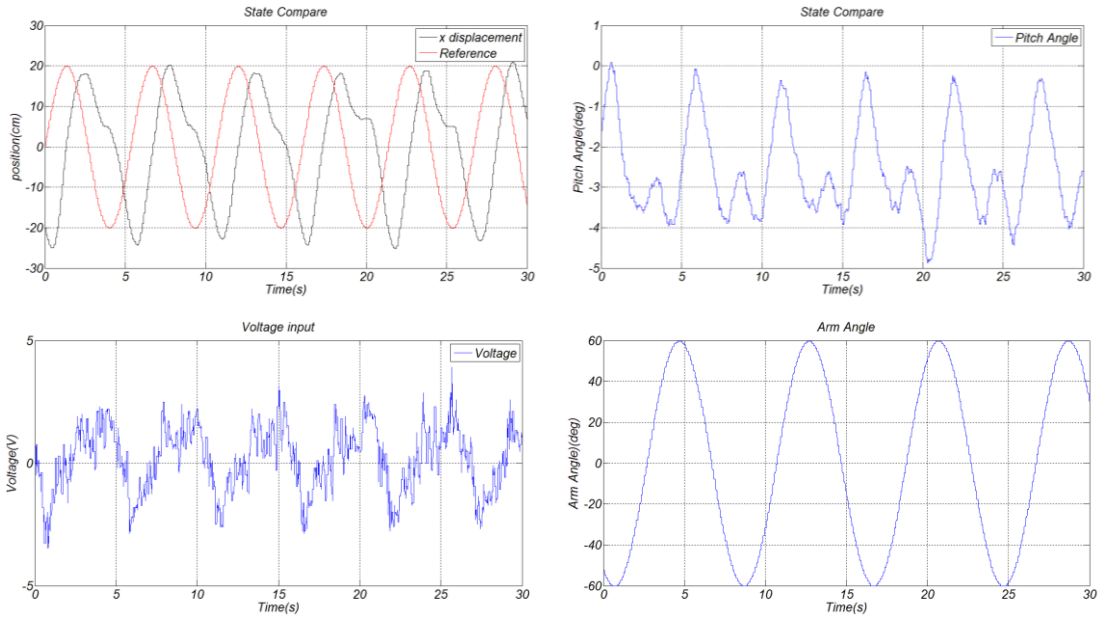

Figure 62: Sinusodial type reference without arm disturbance in real time

Sinusoidal reference also gives good results. Voltage input is under limits.

6.3 Real Time Experiments with 50 g Loaded Arm is Affecting as Disturbance

In this subsection there is disturbance as arm self inertia and a 50 g weight loaded at the end of arm.

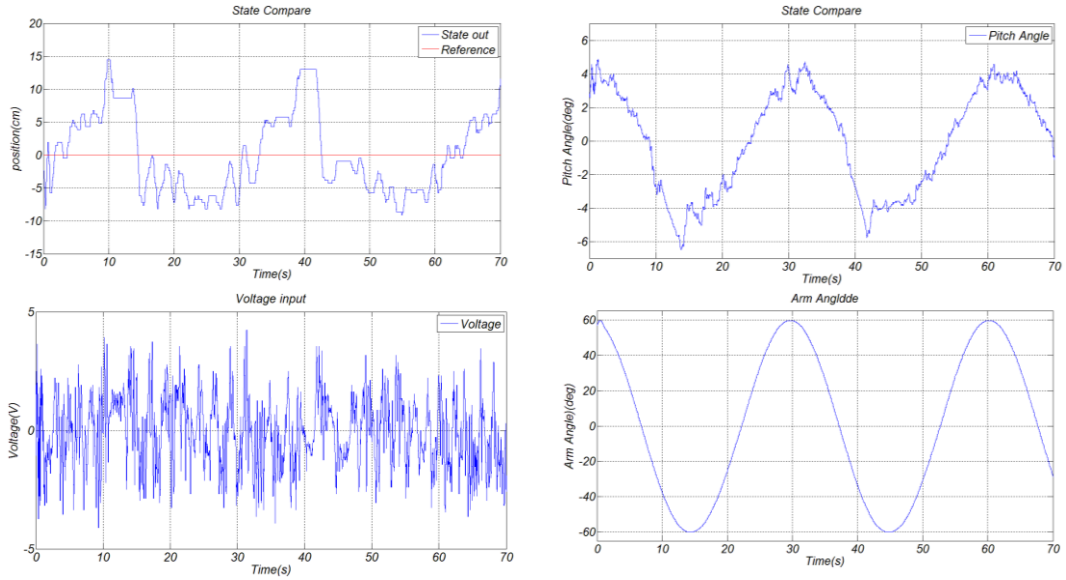

Figure 63: Zero reference with 50 g loaded arm affecting as disturbance in real time

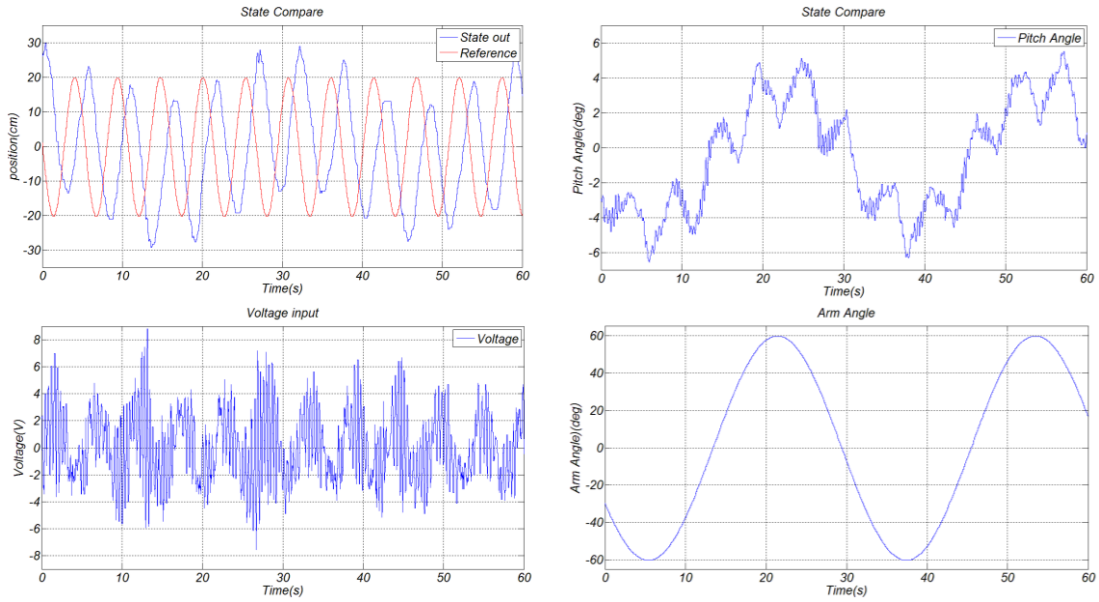

Figure 64: Sinusodial type reference with 50 g loaded arm affecting as disturbance in real time

It is clearly seen in Figure 63 and 64 that CDM controller is eliminates disturbances and ensures the stability conditions.

CHAPTER 7

DISCUSSIONS AND CONCLUSIONS

Two wheeled inverted pendulum robot observed given different types of references. In simulations disturbances applied to the system and stability performance observed. CDM controller take places in polynomial control method and state feedback structure can be used. This controller method is effortless in terms of choosing state feedback gain. One can easily determine the relation between time settling time and parameters of stability index. Also Standart Manabe form ensures the easiest way to choose state feedback gain. Stability index determines the stability performance of the system and coefficient diagram show us easily to choose robust parameters.

In simulations arm helps eliminating the disturbances. Results show us CDM controller is good at choosing appropriate parameters and obtaining right state feedback gains. Also Standart Manabe forms help user to choose easy way of optimizing gains. It is clearly seen in figure that without arms disturbances are not completely eliminated. But Condition with arm results give satisfying results

In Real time experiments arm as a disturbance source observed and tracking and disturbance capability observed. Figures show us CDM controller succeeded in eliminating disturbances.

Two dimensional system is observed in this thesis. Effect of the arm studied while the controller rejects disturbances. In future arm effect on to the system posture stability will be studied.

REFERENCES

1. Acar C., 2008, “A Robust Control of Two-Wheeled Mobile Manipulator with Underactuated Joint by Nonlinear Backstepping Method”, M.Sc Thesis, Keio University, Japan.
2. Acar C., Murakami T., 2010, “Motion Control of Dynamically Balanced Two-Wheeled Mobile Manipulator through CoG Manipulation”, The 11th IEEE International Workshop on Advanced Motion Control, pp.715-720, Nagaoka, Japan.
3. Acar C., Murakami T., 2008, “Underactuated Two-Wheeled Mobile Manipulator Control Using Nonlinear Backstepping Method”, IEEE, pp. 1680-1685.
4. O. Brock, O. Khatib, and S. Viji , 2002 ,“Task-Consistent Obstacle Avoidance and Motion Behavior for Mobile Manipulation”, IEEE International on Robotics and Automation, vol.1,pp.388-393.
5. K. Nagatani, and S. Yuta, 1996, “Designing Strategy and Implementation of Mobile Manipulator Control System for Opening Door”, IEEE International on Robotics and Automation, vol.3, pp.2828-2834., Minneapolis.
6. Küçük D., 2010, “Design of Two-Wheeled Twin Rotored Hybrid Robotic Platform”, M.Sc Thesis, Atılım University, Ankara .
7. Göçmen A., 2011, “Design of Two Wheeled Electric Vehicle” ,M.Sc Thesis, Atılım University, Ankara .
8. Nguyen H.G, Morrell J., Mullens K., Burmeister A., Miles S., Farrington N., Thomas K., Gage D. W. , 2004, ”Segway Robotic Mobility Platform”, Mobile Robots XVII, Philadelphia, PA.
9. S. M. Goza, R. O. Ambrose, M. A. Diftler and I. M. Spain, 2004, “Telepresence Control of the NASA/DARPA Robonaut on a Mobility Platform”, Proceedings of the SIGCHI Conference on Human Factors in Computing Systems, pp.623-629.

10. B. J. Thibodeau, P. Deegan, and R. Grupen “Static analysis of contact forces with a mobile manipulator”, Robotics and Automation, 2006. ICRA 2006. Proceedings 2006 IEEE International Conference, May 2006, pp. 4007-4012, 2006.
11. M. C. Martin “Controlling Cardea: Fast Policy Search in a High Dimensional Space”, MIT Media Laboratory, Vision and Modelling Technical Report, no.583, June 2004.
12. J. Searock, B. Browning, and M. Veloso, “Segway CM-RMP Robot Soccer Player,” Proc. RoboCup International Symposium,Lisbon, Portugal, July 2004.
13. B. Browning, P. Rybski, J. Searock, and M. Veloso, “Development of a soccer-playing dynamically-balancing mobile robot,” Proc. Int. Conf. on Robotics and Automation (ICRA'04),New Orleans, LA, April-May 2004.
14. B. Browning, L. Xu, and M. Veloso, “Skill acquisition and use for a dynamically-balancing soccer robot,” Proc. 19th Nat. Conf. on Artificial Intelligence (AAAI'04),San Jose, CA, July 2004.
15. A. Howard, D. F. Wolf, and G. S. Sukhatme, “Towards 3D Mapping in Large Urban Environments,” IEEE/RSJ Int. Conf. on Intelligent Robotsand Systems (IROS’04),Sendai, Japan, September 2004.
16. F. Grasser, A. D’ Arrigo, S. Colombi, and A. Rufer, “JOE: a mobile, in verted pendulum, ” IEEE Transactions on industrial electronics, vol. 49, no. 1, pp. 107–114, 2002.
17. P. Deegan, B. Thibodeau, and R. Grupen, “Designing a self-stabilizing robot for dynamic mobile manipulation,” in Robotics: Science and Systems-W orkshop on Manipulation for Human Environments, 2006.
18. T. Lauwers, G. Kantor, and R. Hollis, “A dynamically stable single wheeled mobile robot with in verse mouse-ball drive”, IEEE International Conference on Robotics and Automation, 2006, pp. 2884–2889
19. Kuindersma S., Grupen R., Barto A., 2011 “Learning Dynamic Arm Motions for Postural Recovery”, IEEE-RAS International Conference on Humanoid Robots, pp 7-12, Bled, Slovenia.
20. Stillman M., Olson J., Gloss W., 2010, “Golem Krang: Dynamically Stable Humanoid Robot for Mobile Manipulation”, ICRA’10 International Conference on Robotics And Automation.

21. Stillman M, Wang J., Teeyapan K., Marceau R., 2009, “Optimized Control Strategies for Wheeled Humanoids and Mobile Manipulators”, IEEE-RAS International Conference on Humanoid Robotics, Paris, France
22. R. Grepl, 2009, “Balancing Wheeled Robot: Effective Modelling, Sensory Processing And Simplified Control”, Engineering Mechanics, Vol. 16, No. 2, pp. 141–154.
23. Y. Takita, H. Date and H. Shimazu, 2009, “Competition of Two-wheel Inverted Pendulum Type Robot Vehicle on MCR Course”, The 2009 IEEE/RSJ International Conference on Intelligent Robots and Systems October 11-15 2009, pp. 5579-5584, St. Louis, USA.
24. L. J. Butler and G. Bright, 2008, “Feedback Control of a Self-balancing Materials Handling Robot”, 2008 10th Intl. Conf. on Control, Automation, Robotics and Vision, 17–20 December 2008, pp. 274-278, Hanoi, Vietnam.
25. G. Chi, J. Hausbach and B Hunter, 2005, “Segbot”, Senior Design Project, University of Illinois at Urbana-Champaign, USA.
26. J. Solis, R. Nakadate, Y. Yoshimura, Y. Hama and A. Takanishi, 2009, “Development of the Two-Wheeled Inverted Pendulum Type Mobile Robot WV-2R for Educational Purposes”, The 2009 IEEE/RSJ International Conference on Intelligent Robots and Systems, October 11-15 2009, pp. 2347-2352, St. Louis, USA.
27. S. Jeong and T. Takahashi, 2007, “Wheeled Inverted Pendulum Type Assistant Robot: Inverted Mobile, Standing, and Sitting Motions”, Proceedings of the 2007 IEEE/RSJ International Conference on Intelligent Robots and Systems, Oct 29 - Nov 2 2007, pp. 1932-1937, San Diego, CA, USA.
28. C. N. Huang, 2010, “The Development of Self-Balancing Controller for OneWheeled Vehicles”, Scientific Research Journals of Engineering, Vol 2, pp.212-219.
29. P. Oryschuk, A. Salerno, A. M. Al-Husseini and J. Angeles, 2009, “Experimental Validation of an Underactuated Two -Wheeled Mobile Robot”, IEEE/ASME Transactıons on Mechatronıcs, Vol. 14, No. 2, April 2009, pp. 252-257.

30. A. Blankespoor and R. Roemer, 2004, “Experimental Verification of the Dynamic Model for a Quarter Size Self-Balancing Wheelchair”, Proceeding of the 2004 American Control Conference, June 30 - July 2 2004, pp. 488-492, Boston, Massachusetts, USA.
31. X. Ruan and J. Zhao, 2008, “The PWM Servo and LQR Control of a Dual-wheel Upright Self-balancing Robot”, 2008 International Symposiums on Information Processing, pp. 586-590.
32. S. W. Nawawi, M. N. Ahmad and J. H. S. Osman, 2008, “Real-Time Control of a Two-Wheeled Inverted Pendulum Mobile Robot”, World Academy of Science,Engineering and Technology, Issue 39, pp. 214-220
33. A. T. Becker, 2008, “Mobile Robot Motion-Planning Using Wireless Signals For Localization”, M.Sc., Graduate College of the University of Illinois at Urbana-Champaign, USA.
34. S. C. Lin and C. C. Tsai, 2009, “Development of a Self-Balancing HumanTransportation Vehicle for the Teaching of Feedback Control”, IEEE Transaction on Education, Vol. 52, No. 1, February 2009, pp. 157-168.
35. Y. Kim, S. H. Kim and Y. K. Kwak, 2006, “Improving Driving Ability for a Two-Wheeled Inverted-Pendulum-Type Autonomous Vehicle”, Proceedings of the IMechE Part D Journal of Automobile Engineering, Vol. 220, No. 2, pp. 165-175.
36. K. C. R. Ho, 2005, “Balancing Wheeled Robot”, Research Project, University of Southern Queensland, Australia.
37. M. Kumaga and T. Ochiai, 2009, “Development of a Robot Balanced on a Ball”, 2009 IEEE International Conference on Robotics and Automation, May 12-17 2009, pp. 4106-4111, Japan.
38. U. Nagarajan, A. Mampetta, G. A. Kantor and R. L. Hollis, 2009, “State Transition, Balancing, Station Keeping, and Yaw Control for a Dynamically Stable Single Spherical Wheel Mobile Robot”, 2009 IEEE International Conference on Robotics and Automation, May 12-17 2009, pp. 998-1003, Japan.
39. T. Hu, H. Zhang, X. Dai, X. Xai, R. Liu and B. Qiu, 2007, “Design and Implementation of Self-Balancing Coaxial Two Wheel Robot Based on HSIC”, Proceeding of SPIE, Volume 6794, 6794H-1-9.

40. A. Salerno and J. Angeles, 2007, “A New Family of Two-Wheeled Mobile Robots: Modeling and Controllability”, IEEE Transaction on Robotics, Vol. 23, No. 1, February 2007, pp. 169-173.
41. K. Pathak, J. Franch and S. K. Agrawal, 2005, “Velocity and Position Control of a Wheeled Inverted Pendulum by Partial Feedback Linearization”, IEEE Transactıons on Robotıcs, Vol. 21, No. 3, June 2005, p. 505-513.
42. K. M. Goher and M. O. Tokhi, 2010, “Development, Modeling and Control of a Novel Design of Two-Wheeled Machines”, Cyber Journals Multidisciplinary Journals in Science and Technology, Journal of Selected Areas in Robotics and Control (JSRC), December Edition.
43. W. Zhou, 2008, “Platform for Ergonomic Steering Methods Ġnvestigation of "Segway-Style" Balancing Scooters”, M.Sc. Thesis, University of Waikato, New Zealand.
44. M. Burkert, T. Groll, T. Lai, T. McCoy and D. Smith, 2004, “Segway Design Project”, Project Report, Grand Valley State University The Padnos School of Engineering, USA.
45. C. C. Tsai, C. K. Chan and Y. H. Fan, 2008, “Planned Navigation of a Selfbalancing Autonomous Service Robot”, IEEE International Conference on Advanced Robotics and Its Social Impacts, Aug. 23-25 2008, Taipei, Taiwan.
46. H. Tirmant, M. Baloh, L. Vermeiren, T. M. Guerra and M. Parent, 2002, “B2, An Alternative Two Wheeled Vehicle for an Automated Urban Transportation System”, IEEE Intelligent Vehicle Symposium, June 17-2 2002, pp. 594-603
47. P. Pannil, A. Klaeoyotha, P. Ukakimaparn, T. Trisuwannawat, K. Tirasesth and N. Kominet, 2008, “Development of Inverted Pendulum System at KMITL”, 2008 International Symposium on Communications and Information Technologies, pp. 389-393.
48. J. S. Hu, M. C. Tsai, F. R. Hu and Y. Hori, 2010, “Robust Control For Coaxıal Two-Wheeled Electrıc Vehıcle”, Journal of Marine Science and Technology, Vol. 18, No. 2, pp. 172-180.
49. S. Bouabdallah and R. Siegwart, 2005, “Backstepping and Sliding-mode Techniques Applied to an Indoor Micro Quadrotor”, Proceedings of the

2005 IEEE International Conference on Robotics and Automation, pp. 2259-2264, Barcelona, Spain.

50. G. V. Raffo, M. G. Ortegaand, F. R. Rubio, 2008, “Backstepping/Nonlinear H∞ Control for Path Trackingof a QuadRotor Unmanned Aerial Vehicle”, American Control Conference, pp. 3356-3361, Westin Seattle Hotel, Seattle, Washington, U.S.A.
51. F. Kendoul, I. Fantoni, R. Lozano, 2005, “Modeling and control of a small autonomous aircraft having two tilting rotors”, Proceedings of the 44th IEEE Conference on Decision and Control, and the European Control Conference, pp.8144-8149, Seville, Spain.
52. Budiyono, S. S. Wibowo, 2007, “Optimal Tracking Controller Design for a Small Scale Helicopter”, Journal of Bionic Engineering 4, pp. 271−280.
53. C. H. Chiu and Y. F. Peng, 2006, “Design and Implement of the Self-Dynamic Controller for Two-Wheel Transporter”, 2006 IEEE International Conference on Fuzzy Systems, July 16-21 2006, pp. 480-483, Vancouver, BC, Canada.
54. H. J. Jean and C. K. Wang, 2009, “Design And Implementatıion Of A Balancing Controller for Two-Wheeled Vehicles Using A Cost-Effective MCU”, Proceedings of the Eighth International Conference on Machine Learning and Cybernetics, July 12-15 2009, pp. 3329-3334, Baoding, China.
55. S. C. Lin, C. C. Tsai and W. L. Lou, 2007, “Adaptive Neural Network Control of a Self-balancing Two-wheeled Scooter”, The 33rd Annual Conference of the IEEE Industrial Electronics Society (IECON), Nov. 5-8 2007, pp. 868-873, Taipei, Taiwan.
56. S. C. Lin, C. C. Tsai and H. C. Huang, 2009, “Nonlinear Adaptive Sliding-Mode Control Design for Two-Wheeled Human Transportation Vehicle”, Proceedings of the 2009 IEEE International Conference on Systems, Man, and Cybernetics, October 2009, pp.1965-1970, San Antonio, TX, USA.
57. D. Choi and J. H. Oh, 2008, “Human-friendly Motion Cont rol of a Wheeled Inverted Pendulum by Reduced-order Disturbance Observer”, 2008 IEEE International Conference on Robotics and Automation, May 19-23 2008, pp. 2521-2526, Pasadena, CA, USA.
58. J. Li, X. Gao, Q. Huang, Q. Du and X. Duan, 2007, “Mechanical Design and Dynamic Modeling of a Two-Wheeled Inverted Pendulum

Mobile Robot", Proceedings of the IEEE International Conference on Automation and Logistics, August 18 – 21 2007, pp. 1614-1619, Jinan, China.

59. M. Sasaki, N. Yanagihara, O. Matsumoto and K. Komoriya, 2005, "Steering Control of the Personal Riding-type Wheeled Mobile Platform (PMP)", 2005, IEEE/RSJ International Conference on Intelligent Robots and Systems, pp.1697-1702.
60. S. Manabe, "Coefficent Diagram Method", IFAC Automatic Control in Aerospace, Seoul, Korea, 1998.
61. S. Manabe, "Application of Coefficent Diagram Method to MIMO Design in Aerospace, 15th Triennial World Congress, Barcelona, Spain, 2002.
62. A, I. Cahyadi, D. Isarakorn, T. Benjanarasuth, J. Ngamwiwit and N. Komine, "Application of Coefficient Diagram Method for Rotational Inverted Pendulum Control", 2004 8th International Conference on Control, Automatlon, Robotics and Vision, pp. 1769-1773, Kunming, China, 69th December 2004.
63. E. Asa, T. Benjanarasuth, J. Ngamwiwit , N. Komine, "Hybrid Controller for Swinging up and Stabilizing the Inverted Pendulum on Cart", International Conference on Control, Automation and Systems, pp. 2504-2507, Seoul, Korea, October 2008.
64. R.Hirokawa, K. Sato, "Autopilot Design for a Missile with Reaction-Jet Using Coefficient Diagram Method", AIAA Guidance, Navigation and Control Conference and Exhibit, Montreal Canada, August 2001.
65. S. Manabe, "Coefficent Diagram Method as Applied to the Attitude Control of Controlled-Bias-Momentum Satellite", 13th IFAC Symposium on Automatic Control in Aerospace, pp. 322-327, California, USA, September 1994.